Petrogenesis of High Heat Producing Granite: Implication for Mt Painter Province, South Australia

Kamonporn Kromkhun, (M.Sc)

Geology and Geophysics
School of Earth & Environmental Science
University of Adelaide

Thesis submitted for the degree of Doctor of Philosophy
in the Faculty of Science, University of Adelaide

January 2010

Chapter 1 Overview

Granite is the most abundant rock type in continental crust and typically contains higher concentrations of radioactive elements (U, Th and K) than other rock types (Table 1.1; Haenel et al., 1988; Royden, 1991). Heat production values per unit value (*A*) can be calculated from the equation of Rybach (1988);

$A = p(9.52c_U+2.56c_{Th}+3.48c_K)\ 10^{-5}$

P Density in kg/m^{-3}

C_U Uranium concentration in ppm

C_{Th} Thorium concentration in ppm

C_K Potassium concentration as a percentage

Granites typically contain heat production values ranging between 2-20 μWm^{-3} with an average of 2.53 μWm^{-3} (Table 1.1; Haenel et al., 1988). Some granites are documented to contain unusually high concentrations of radioactive elements leading to high values of heat production. In this study, granites with heat production values more than 5 μWm^{-3} are classified as High Heat Producing Granites (HHP Granites).

High Heat Producing granites are economically important because of their association with some ore deposits and their potential for geothermal energy. For example, uranium deposits are often found near HHP granite provinces such as Mt Painter Province, South Australia (Coats and Blissett, 1971), the Gabal Ribdab Area, Southeast Desert Egypt (Ibrahim et al., 2001) and the Streltsovka, Russia (Chabiron et al., 2003). Some tin deposits are also related to HHP granites such as the Lake District, UK (Plant et al., 1986) and the Patinga Mine, Brazil (Lenharo et al., 2003). HHP granites may also provide the heat source for explorable geothermal energy resources. Studies of possible geothermal resources are now developing in South Australia and Europe (Hurter et al., 2003). However, the genesis of HHP granites has not been studied in detail. The questions of why and how the granites contain unusually high U, Th and K concentrations have not been satisfactorily answered.

The radioactive elements, U, Th and K, are mostly concentrated in upper continental crust (Table 1.2). These elements are compatible with partial melts, which leads to high U, Th and K concentrations within more evolved rocks (Rudnick and Fountain, 1995). Thesse evolved rocks tend to occurred at shallow depth in the crust. Therefore there is a generak trend for decreasing U, Th and K concentrations with increasing depth in the crust.

Table 1.1 Average heat production of some rock types.

Lithology	U (ppm)	Th (ppm)	K (wt%)	A (μWm^{-3})
Granite/Rhyolite	3.9	16	3.6	2.53
Granodiorite/Dacite	2.3	9	2.6	1.51
Diorite/Andesite	1.7	7	1.1	1.06
Gabbro/Basalt	0.5	1.6	0.4	0.29
Peridotite	0.02	0.06	0.006	0.01
Undepleted mantle	0.02	0.09	0.02	0.01
Ocean Island Basalt	1.02	4	1.2	0.67
Limestone	2.0	1.5	0.3	0.66
Shales and siltstone	3.7	12	2.7	2.1
Quartzite	0.6	1.8	0.9	0.37

Note: heat production values based on U, Th and K from Haenel et al., 1988

Table 1.2 Average U, Th and K concentrations of main lithospheric reservoirs.

	U (ppm)	Th (ppm)	K_2O (wt%)	A (μWm^{-3})	Source
Bulk crust	1.3	5.6	1.81	0.91	Kemp and Hawkesworth, 2003
Upper crust	2.7	10.5	2.80	1.71	Kemp and Hawkesworth, 2003
Middle crust	1.3	6.5	2.30	1.02	Kemp and Hawkesworth, 2003
Lower crust	0.02	1.2	0.61	0.15	Kemp and Hawkesworth, 2003
Depleted peridotites	0.006	0.04	0.01	0.01	Fowler, 1990
Undepleted mantle	0.02	0.1	0.02	0.01	Fowler, 1990
Chondritic meteorites	0.013	0.04	0.078	0.01	Turcotte and Schubert, 1982

1.1 Granite classification

Granites have been classified according to criteria such as the assumed petrogenesis, mineralogy, geochemistry and tectonic setting. Examples are; alphabetic classification (S-, I-, A-, C- and M-type granites; Chappell and White, 1974; Kilpatrick and Ellis, 1992), magnetite- and ilmenite-series granites (Ishihara, 1977), R1-R2 discrimination diagrams (De la Roche et al., 1980), trace element discrimination diagrams (Pearce et al., 1984) and Fe number, modified alkali-lime index (MALI) and aluminum saturation index

(ASI; Frost et al., 2001). However, none of these granite classification schemes is based on U, Th and K elements, and thus HHP granites have not yet been independently classified and may in fact transgress other classifications. However most HHP granites are evolved calc-alkaline intrusions emplaced late in orogenic cycles and are alkaline-subalkaline (Plant et al., 1984), they are most typically a subtype of the A-type granite group (Table 1.3). Moreover, definitions of A-type granites that are based on petrochemical and geochemical criteria are granites characterised by high LILEs (Large Ion Lithophile Elements) and HFSEs (High field strength elements) abundances and alkali-calcic to alkalic compositions.

Table 1.3 Characteristics of S-, I- and A type granites.

Granite type	Tectonic environment	Chemical signature	Typical minerals
S-type	Orogenic	Metaluminous to strongly peraluminous, high $^{18}O/^{16}O$, $^{87}Sr/^{86}Sr$	Muscovite, garnet, cordierite, tourmarine
I-type	Orogenic	Metaluminous	Biotite, hornblende
A-type	Anorogenic, rift-related	Metaluminous to mildly peralkaline, Fe-enriched, high LILE and HFSE	Fe-biotite, Na-amphibole, Na-pyroxene, hedenbergite, fayalite, titanite

1.2 A-type granites

The A-type granite category was firstly defined by Loiselle and Wones (1979) to describe granites that have an alkaline composition, contain anhydrous minerals, crystallized under low oxygen fugacity and emplaced in intraplate or anorogenic settings. Since the introduction of the term A-type granite, numerous studies have discussed their petrography, geochemistry, sources characteristics, the role of fluids, isotopic signatures, petrogenesis and tectonic settings. The results show that the category A-type granite has diverse rock types, compositions and tectonic settings and may involve multiple processes.

Most A-type granites are characterised by high K_2O, Fe/(Fe+Mg), and Rb/Sr, enriched high field strength elements (e.g. Zr, Hf, Nb and Ta) and depleted Ca, Ba, Sr and Eu (King et al., 2001). Several genesis models of A-type granites have been proposed, which involve crustal and mantle sources, including; fractionation of mantle-derived magma, low degrees of partial

melting of lower-crustal granulite, anatexis of undepleted I-type tonalitic crustal sources and metasomatism of granitic magma (Jung et al. 1998 and references therein). These granitic rocks have been recognized to have formed in a variety of within-plate and late to post orogenic settings (Eby, 1992). A-type granites are distributed throughout the geological times; however they are more abundant in the Proterozoic period (Kemp and Hawkesworth, 2003). Most of these granitic rocks are coeval with mafic intrusions that suggest some components of mantle input.

1.3 High Heat Producing Granites

High K, Th and U granites are named according to their mineralogy and mineral proportions including biotite granite, alkali granite, monzogranite, albite granite, rapakivi granite and topaz granite. HHP granites may be pink, red, white and grey, with variable grain size (fined- to coarse-grained). They are mainly composed of quartz, coarsely perthitic alkali feldspar, plagioclase, biotite, microcline, microperthite and Fe-hornblende, and contain accessory zircon, titanite, allanite, apatite, thorite, Th-rich uranitite, chevkinite, epidote, monazite, fluorite and magnetite. HHP granites are generally leucocratic and typically exhibit porphyritic, granophyric or rapakivi textures with some seriate textures. The granites are characterised by high SiO_2 (up to 78 wt%) and K_2O compositions, and low levels of CaO, MgO, P_2O_5, Al_2O_3, Fe_2O_3 and MgO. These characteristics of HHP granites are also observed in tin granites (Tischendorf, 1977). They are high-K granitiods with high alkali content and K_2O/Na_2O ratios. HHP granites generally have high abundances of many trace elements (e.g. Rb, U, Th, Zr and Ga), high HFSE, enriched in F, depleted in P and have high Ga/Al and Rb/Sr ratios and negative Eu anomalies. Types of HHP granites are divided by their petrographic, mineralogical and geochemical characteristics. They are mainly metaluminous with some peraluminous to mildly peralkaline. The low P_2O_5 content can be used to classify the granites as a subtype of topaz granites (Taylor, 1992). Most HHP granites show mineralogical and petrographic characteristics that correspond to within-plate granites on tectonic discrimination diagrams using Rb and Y+Nb data (Pearce et al., 1984). They are commonly emplaced during the late stage of an orogenic event and in

anorogenic settings (Bonin, 1987; Nardi and Bonin, 1991) and may be associated with extensional fracture systems (Lenharo et al., 2002).

1.4 Distribution of High Heat Producing Granite

Based on definition of HHP granites containing heat production values more than 5 μWm^{-3}, HHP granites are found in Archaean, Proterozoic and Phanerozoic terranes; however most are Proterozoic in age (Figure 1.1), with examples being found in Asia, Australia, Europe, North America, South America, Africa and Antarctica (e.g. Sandiford et al., 2002; Haapala and Lukkari, 2005; Vander Auwera et al., 2003; Peterson et al., 2002; Liu, et al., 2006).

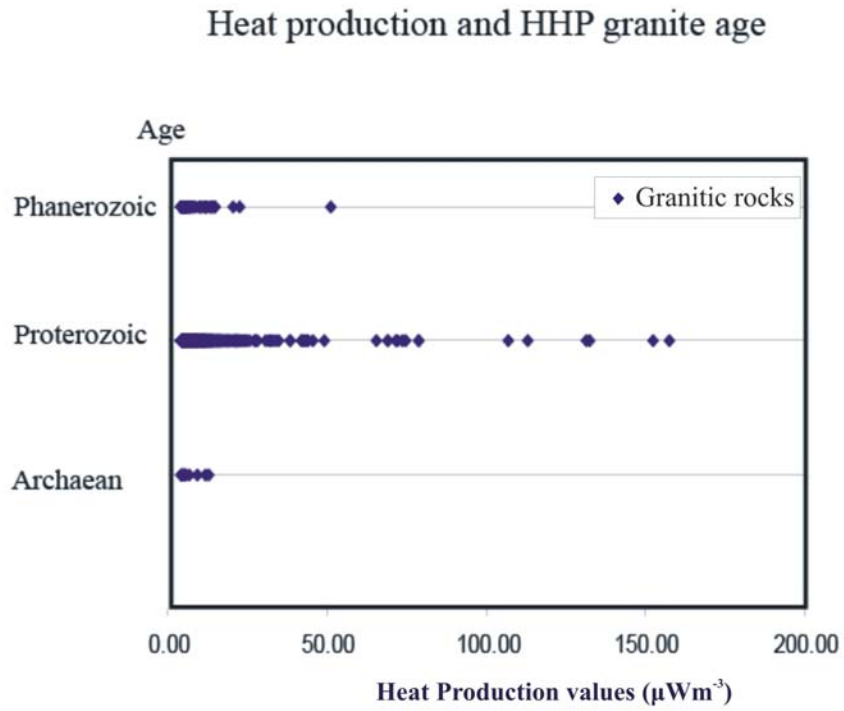

Figure 1.1 Heat Production values versus age diagram (data from published papers complied by Kromkhun, 2006).

1.4.1 Asia

HHP granites of Asia are found in India and China. In eastern China and Inner Mongolia, HHP granites occur within the Central Asian Orogenic belt (e.g. Qui, et al, 2004; Lui et al, 2005). The HHP granites (heat production up to ~8 μWm^{-3}) of Zhejiang and Fujian Provinces in SE China are Late Cretaceous in age (Qui, et al, 2004). NE China granites range in age from

Permian to early Cretaceous and normally do not have very high heat production (<4 μWm^{-3}, with the highest at 6 μWm^{-3}; Wu et al, 2002). In Northern Inner Mongolia, HHP granites show heat producing from 4 to 15 μWm^{-3} and their ages range from 149-111 Ma (Lui et al, 2005).

HHP granites in India are found in the Dharwar craton, Rajasthan and eastern Singbhum and have ages ranging from Achaean to Mezoproterozoic with heat production up to 13 μWm^{-3} (Kumar and Reddy, 2004; Misra et al., 2002; Pandit and Khatatneh, 1998; Chaudhri et al., 2003).

1.4.2 Africa

In Africa, HHP granites have been reported from Egypt, South Africa, Ethiopia, Nigeria and Namibia, with ages ranging from Phanerozoic to Proterozoic. The Proterozoic Egyptian HHP granites are found in Gabal El Fereyid and South Eastern Desert areas with the Arabo-Nubian Shield belt (Adb El-Naby and Saleh, 2003; Abbady et al., 2006). They normally have high uranium (up to 30 ppm) and low Th (up to 23 ppm) contents (Adb El-Naby and Saleh, 2003; Abbady et al., 2006). Neoproterozoic HHP granites in South Africa occur in the southwestern Saldania belt of the Western Cape Province (Scheepers, 1995). The uranium and thorium concentrations are correlated and they have a heat production average of 5 μWm^{-3} with the highest being 12 μWm^{-3} (Scheepers, 1995). In Namibia, HHP granites are found in central western Namibia and are known as the anorogenic Damalaland and Gross Spitzkoppe granites (Frindt et al., 2004). They are early Creataceous in age, with high radioactivity biotite granites having heat production up to 22 μWm^{-3}, with an average of 5 mWm^{-3}. The Nigerian HHP granites emplaced in the Cretaceous are known as Arfvedsonite granites. They are prevalent in the northern sector of the Nigerian anorogenic ring-complex province (Ogunleye et al., 2005) and are niobium- and uranium-rich granites, with heat production up to 51 μWm^{-3} (Ogunleye et al., 2005).

1.4.3 North America

Proterozoic HHP granites of North America are reported from Wyoming and central Colorado in the USA and from Canada. They have an average heat production of 5 μWm^{-3}. The 1.43 Ga Red Mountain monzonitic

granite of Wyoming is a Th-enriched HHP granite with heat production up to 8 μWm^{-3} (Anderson et al., 2003). In Colorado, the 1.08 Ga Pikes Peak anorogenic granites commonly show low heat production values; however fayalite-bearing granites show heat production values up to 6 m μWm-3 (Smith et al, 1999). The PalaeoproterozoicTrans-Hudson granites and associated volcanic rocks in Canada have average heat production values of 7 μwm^{-3} with average U, Th and K_2O of 8 ppm, 56 ppm and 5 wt% (Peterson et al., 2002).

1.4.4 South America

In South America, Proterozoic HHP granites have mainly been reported from the Amazonian and Sao Francisco Cratons within Brazil (e.g. Agnol and de Oliveira, 2007; Costi et al., 2002; Juliani et al., 2002; Lenharo et al., 2003). They are found in the Pitinga, the Goias areas of the Amazonian Craton in Northern Brazil and along the border of the Sao Francisco craton in northeast Brazil. The Pitinga Mine granites (2.2-2.4 Ga) show extremely high radioactive element contents (U content up to 499 ppm and Th content up to 864 ppm) with heat production values up to 157 μWm^{-3} (Lenharo et al., 2003). As a group, they comprise biotite granite, hornblende granite, rapakivi and topaz-bearing granite (Lenharo et al., 2002; 2003) and they are associated with greisen-, skarn-, and vein-type Sn (W-Be-Zn-Pb-Ag) mineralization. The Goias HHP granites have lower heat production values than the Patinga granites. The HHP granites of the Sao Francisco craton were intruded during the Transamazonian cycle (~2.0 Ga) and have an average heat production of 5 μWm^{-3} (Pla Cid et al., 2000).

1.4.5 Europe

In Europe, Proterozoic HHP granites have been reported within the Fennoscandian Shield of Norway, Finland and Poland. In southern Norway, the HHP granites have heat production values up to 9 μWm^{-3} and show high Th contents (Vander Auwera et al., 2003). The Wiborg granites (age of 1.65-1.63 Ga) of Finland that have high heat production (heat production up to 17 μWm^{-3} with average 8 μWm^{-3}) are rapakivi and topaz granites (Haapala and Lukkari, 2005). Ferrro-potassic HHP granites of NE Poland include quartz

monzonite, granodiorite and rapakivi-like granites, and were intruded at 1.5 Ga (Skridlaite et al, 2003). They have heat production values up to 12 μWm^{-3} and are characterized by high U and low Th contents. The Cretaceous HHP granites were reported from Turkey and Permian HHP granites from Russia. The Cretaceous HHP granites within Turkey are quartz monzonites and syenite with HP values up to 16 μWm^{-3} with average of 6 μWm^{-3} (Kooksal et al., 2004). They are typically Th-enriched with Th contents up to 121 ppm (Kooksal et al., 2004).

1.4.6 Antarctica

HHP granites in Antarctica are poorly known. The HHP granites of Antarctica are found in the Grove Mountains of East Antarctica an inland continuation of the Pan-African Prydz Belt emplaced during 550 to 500 Ma (Liu, et al., 2006). The granites at the Grove Mountains have heat production up to 11 μWm^{-3} showing Th-riched HHP granites. Liu et al. (2006) suggested that the granitoids of the Grove Mountains were emplaced in the extensional environment of formerly overthickened crust. Proterozoic granites from the Terre Adèlie Craton of Antarctica were collected from debris forming the moraines contain low heat production values (less than 5 μwm^{-3}) with average U, Th and K_2O contents of 3 ppm, 19 ppm and 5 wt%, respectively (Peucat et al., 2002).

1.4.7 Australia

Many Proterozoic granites in Australia (more detail in Chapter 8) have high heat production rates and these are shown in Table 1.4. In particular, the HHP granites of the Mount Painter Province, Northern Flinders Ranges, South Australia have average heat production values of 22 μWm^{-3}, which is approximately five times higher than normal granites. Because of extremely high heat production values of the Mount Painter granites, these granites are selected for detail studies which aim to understand petrogenesis of HHP granites (see Chapters 2-7). Moreover, data from previous studies of Australian regions where HHP granites are presented including Mount Isa Inlier, Gawler Craton, Curnamona Craton (Broken Hill and Olary Domains)

and Arunta Inlier will be compared to the HHP granite of Mount Painter Province (Chapter 8).

Table 1.4 Heat production values, age and U, Th, K_2O contents of granites in Australia (data from Budd et al., 2001)

NOTE:
This table is included on page 9 of the print copy of the thesis held in the University of Adelaide Library.

1.5 Thesis Aims

- To determine a definition and classification of HHP granites and identify their sources and petrogenesis
- To describe the petrology, geochemistry, mineralogy and isotope composition of felsic and mafic igneous rocks from Mount Painter Province,
- To identify the relative timing and petrogenesis relationship between mafic and felsic igneous rocks from the Mount Painter Province
- To define tectonic evolutions of HHP granites and associated rocks from the Mount Painter Province,
- To collate published data on the geochemical, geochronological, isotopic characteristics of HHP granites from Australia to define, classify and demonstrate their tectonic setting

1.6 Structure of Thesis

This thesis is divided into nine chapters;

- Chapter 1; this chapter introduces general characteristics of high heat producing granites and their distribution. Aims of this project and thesis structure are presented in this chapter.

- Chapters 2 to 7 describe and characterize the Mesoproterozoic granites and associated rocks from the Mt Painter Province. These chapters include
    - Chapter 2 summarizes the regional and local geological setting and Mesoproterozoic igneous rock evolution based on previous works at the Mount Painter Province and reports lithology and petrography of felsic igneous rocks (including the Pepegoona Volcanics, Mt Neill, Box Bore, Terrapinna, Wattleowie and Yerila granites and Yerila-associated microgranular enclaves and mafic rocks. This chapter describes their characteristics at outcrop, in hand specimen and thin-section.
    - Chapter 3 presents geochemical characteristics of major and accessory minerals (including feldspar, biotite, amphibole, zircon, allanite, apatite, Ti minerals and U-Th minerals) from the felsic and mafic igneous rocks. Descriptions of physical characteristics of minerals are addressed using hand specimen and thin section samples. The compositions (major and trace elements) of the minerals were analysed using Electron Microprobe (EMP) and LA-ICP-MS at the Adelaide Microscopy Centre, University of Adelaide.
    - Chapter 4 reports ages of the Mount Painter felsic and mafic igneous rocks by in situ chemical U-Pb single zircon ages using LA-ICP-MS at the Adelaide Microscopy Centre derived at the Adelaide Microscopy Centre, University of Adelaide. This chapter also reports zircon morphology and their U and Th contents and summarizes the magmatic evolution of the Mount Painter Mesoproterozoic felsic-mafic igneous rocks, between ~1600 to 1540 Ma.
    - Chapter 5 investigates the geochemistry of felsic and mafic igneous rocks by studying the major, trace element and REE concentrations using XRF and ICP-MS. Rock classifications, the relationship between felsic and mafic rocks, their tectonic setting, and petrogenesis of the Mount Painter rocks will be interpreted from geochemical data from this study together with previous data (e.g., Johnson, 1987; Stewart and Foden, 2001).
    - Chapter 6 provides the radiogenic isotope compositions, including Nd-Sm, Rb-Sr and Pb-Pb of whole rock samples, Pb-U

isotopic compositions of K-feldspar and Hf contents of zircons from selected samples covering the dominant magmatic suites of both mafic and felsic igneous rocks. Possible sources and petrogenetic processes will be interpreted and discussed using data from this study and previous work including whole rock Sm-Nd and Rb-Sr isotopes from Stewart and Foden (2001) and Neumann (2001), and Pb isotope of whole rock and K-feldspar from Neumann (2001). Analyses of whole-rock Nd-Sm, Rb-Sr and Pb-Pb and K-feldspar Pb-U isotopes were undertaken by using TIMS at University of Adelaide and the Hf isotope composition of zircons was analysed by using MC-ICP-MS at GEMOC, University of Sydney.

  - Chapter 7 addresses the petrogenesis of the HHP felsic and mafic igneous rocks of the Mount Painter Province. Possible sources and processes will be discussed and conclusion developed in this chapter. Implications for the tectonic evolution of the HHP felsic-mafic igneous rocks from the Mount Painter Province will be discussed.

- Chapter 8 investigates the distribution of HHP granties from selected terranes of Australia including Mount Isa Inlier, Gawler Craton, Curnamona Craton (Broken Hill and Olary Domains) and Arunta Inlier. A possible petrogenetic and magmatic evolution model for HHP granites for the Australian continent will be discussed by using the geochemical database of Geoscience Australia and published data.

- Chapter 9 presents a petrogenesis of HHP granites and concludes characteristics and a petrogenesis for HHP granites from Mt Painter Province and selected terranes of Australia.

Chapter 2 Geology, Lithology and Petrography of magmatic rocks from Mt Painter Province

The Mt Painter Province is located in the northern Flinders Ranges, approximately 680 kilometres NNE of Adelaide, South Australia (Figure 2.1). It is part of the Curnamona Craton and has had a long history of mineral exploration, particularly for uranium and copper although no major deposit has been discovered. Copper mineralization was discovered in the overlying Adelaidean sedimentary rocks and small secondary lead and zinc mines operated between 1860 and 1920s (Hore et al., 2005). In addition, radium for medical purposes was mined from uranium deposits near Mt Painter in the 1954. Since 1945, South Australia Department of Mines has explored and identified a variety of mineralization types and more recently, epithermal gold and breccias-hosted uranium mineralization has been targeted for exploration. The area is also thought to have potential for geothermal energy, and this has been the focus of recent work by energy companies (www.pir.sa.gov.au/ geothermal).

2.1 Previous work

Early geological studies of the Mt Painter Province focussed on the copper and uranium mineralization of the basement and surrounding Adelaidean sedimentary rocks (e.g. Mawson, 1923; Sprigg, 1954; Campana, 1956). Coats and Blissett (1971) provide the first detailed study of the geology, structure, stratigraphy and economic geology of the Mt Painter Province, focussing on the stratigraphy and timing relationships between the sedimentary and igneous rocks of the basement and the Neoproterozoic cover. Drexel et al. (1993) presented an update on the geochronology, stratigraphy, structural and metamorphic geology of the Mt Painter Province, summarizing the studies of Teale, (1979), Johnson (1980), Thornton (1980); Sheard et al. (1992). The revision and distinction of the basement stratigraphy and geochronology from Teale (1993a) and Teale and Flint (1993) provide a comprehensive overview of the evolution of the Mt Painter Province as it was understood at that time. Many investigations of the Mt Painter Province have been carried out at the University of Adelaide (e.g. Wall, 1995; Neumann,

1996, 2001; Paul, 1998; McLaren, 2001) have added to the understanding of the stratigraphic and tectonic-metamorphic relationships, and geological evolution. Recent workers have studied the relationship between the high heat flow and heat production of the Mt Painter Province and its metamorphic, metasomatic and tectono-thermal history during the Phanerozoic (e.g. Paul et al., 1999; McLaren et al., 2002; Elburg et al., 2001, 2003).

2.2 Geological setting

The Mt Painter Province consists of the Mt Painter and Mt Babbage Inliers (MPI and MBI), two basement inliers located within the northeastern most part of the Adelaide Fold Belt (Figure 2.1). The south-eastern margin of the Mt Painter Province is the Paralana Fault Zone, a long-lived structure that shows signs of movement druing mid-Tertiary (Froster et al., 1994). The Flinders Ranges are adjacent to the Paralana Fault Zone that resulted in the Mt Painter Province thrust contacted over the Curnamona craton (Teasdale, 1993). The Mt Babbage Inlier is separated from the Mt Painter Inlier by the Yudnamutana Trough, a deep depositional trough that formed by a transcurrent fault system, and in which over five kilometres of Neoproterozoic Adelaidean sedimentary rocks were deposited (Johnson, 1980). The basement comprises metasediments deformed and metamorphosed to amphibolite facies during the Paleoproterozic (Teale, 1993a). A number of granitic bodies and associated felsic volcanics subsequently intruded in to the metasediment-dominated basement during the time interval 1580-1550 Ma, which was overlain by Neoproterozoic sedimentary rocks that are part of Adelaide Fold Belt. Both the basement and cover rocks were deformed and metamorphosed during the Delamerian Orogen approximately 515 - 450 Ma and subsequently in the Ordovician (Elburg et al., 2001).

Paul (1998) suggests that there are three main tectono-thermal episodes in the Mt Painter Province. The first episode includes the onset of Palaeoproterozoic metasediment and the onset of Palaeoproterozoic tectonothermal activity. The second episode involves a pause in tectonothermal activity during which the Freeling Heights Quartzite was deposited and accumulated in a Mesoproterozoic thermal event that included the extrusion of HHP volcanic and granitic intrusions. There was then a 700

Myr hiatus before the onset of the third episode which began with the Neoproterozoic rifting and deposition of a thick package of sedimentary rocks of the Adelaide Fold Belt, up to the end of the Delamerian Orogen. Deformation of the Mt Painter Province and Mt Babbage Inliers are similar, however Delamerian folding, which was controlled by pre-existing structural grain, has caused different structural orientation in these two inliers (NE-SW for the Mount Painter Inlier and E-W for the Mt Babbage Inlier; Robertson et al., 1993). Tectonism at ~1550 Ma may have caused N-E trending shearing and the formation of crustal fractures, shear zones and foliation which Late Mesoproterozoic and Neoproterozoic mafic dykes were intruded along (Robertson et al., 1993). The British Empire Granite, normal S-type granites intruded into the Mt Painter Inlier at the end of Delamerian, has crystallization ages of 440-450 Ma (McLaren et al., 2006).

2.3 Mesoproterozoic magmatic rocks

The Mesoproterozoic magmatic province of the Mt Painter Province consists of a high volume of granitic rocks with lesser amounts of felsic volcanic rocks and with minor mafic magmas occurring as enclaves and dykes (Figure 2.2). The older Proterozoic magmatic episode resulted in the extrusion of the Pepegoona porphyritic volcanics, are dated at 1645 Ma using Rb/Sr method (Compston et al., 1966). The second magmatic event occurred between about 1575 and 1560 Ma. During this event, felsic volcanic magmatism formed the Hart Creek rhyolite (1576±2 Ma; Teale, 1993b) and the Gunsight Prospect dacitic tuff (age of 1575±14 Ma; Teale, 1993b). The Mt Neill granite was intruded at 1569±14 Ma (Teale, 1993b) and was altered between 1575 Ma and 1560 Ma; (Stewart and Foden, 2002). The Petermorra porphyritic volcanics of the northern Mt Babbage Inlier have been dated at 1560±3 Ma (Teale, 1993b). Box Bore gneissic granite that yields an age of 1555±15 Ma (Teale et al., 1995) is strongly deformed and altered. The Terrapinna and Wattleowie granites are interpreted to be co-magmatic and occur in the Mount Babbgae Inlier and the northern Mt Painter Inlier, with the former having a crystallization age of 1557±6 Ma (Sheard et al., 1992). The Yerila granite is found only in the Mount Babbage Inlier and has a crystallization age of 1556±6 Ma (Johnson, 1980).

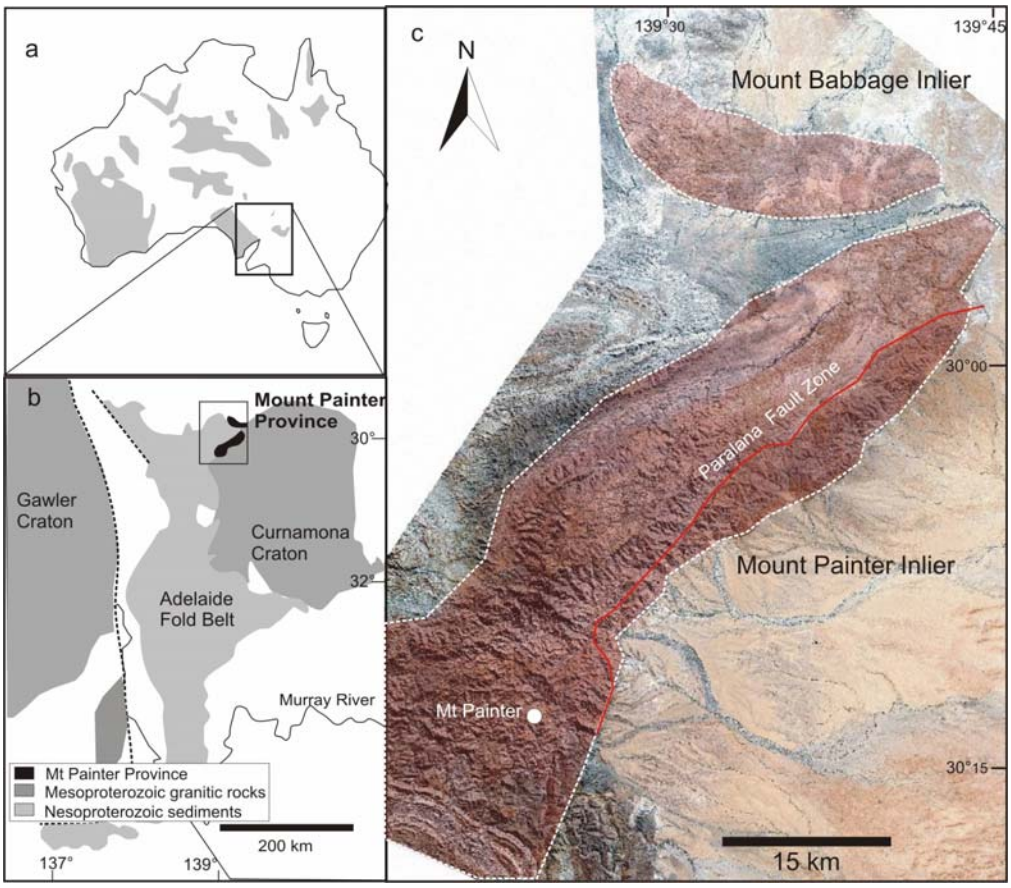

Figure 2.1 Map of the Mt Painter Province consisting of the Mt Painter and Mt Babbage Inliers modified after McLaren et al., 2006; a) major Proterozoic terranes in Australia. Location of b is shown by box, b) simplified geology of South Australia and location of the Mt Painter Province, c) aerial photo of the Mt Painter and Mt Babbage Inliers.

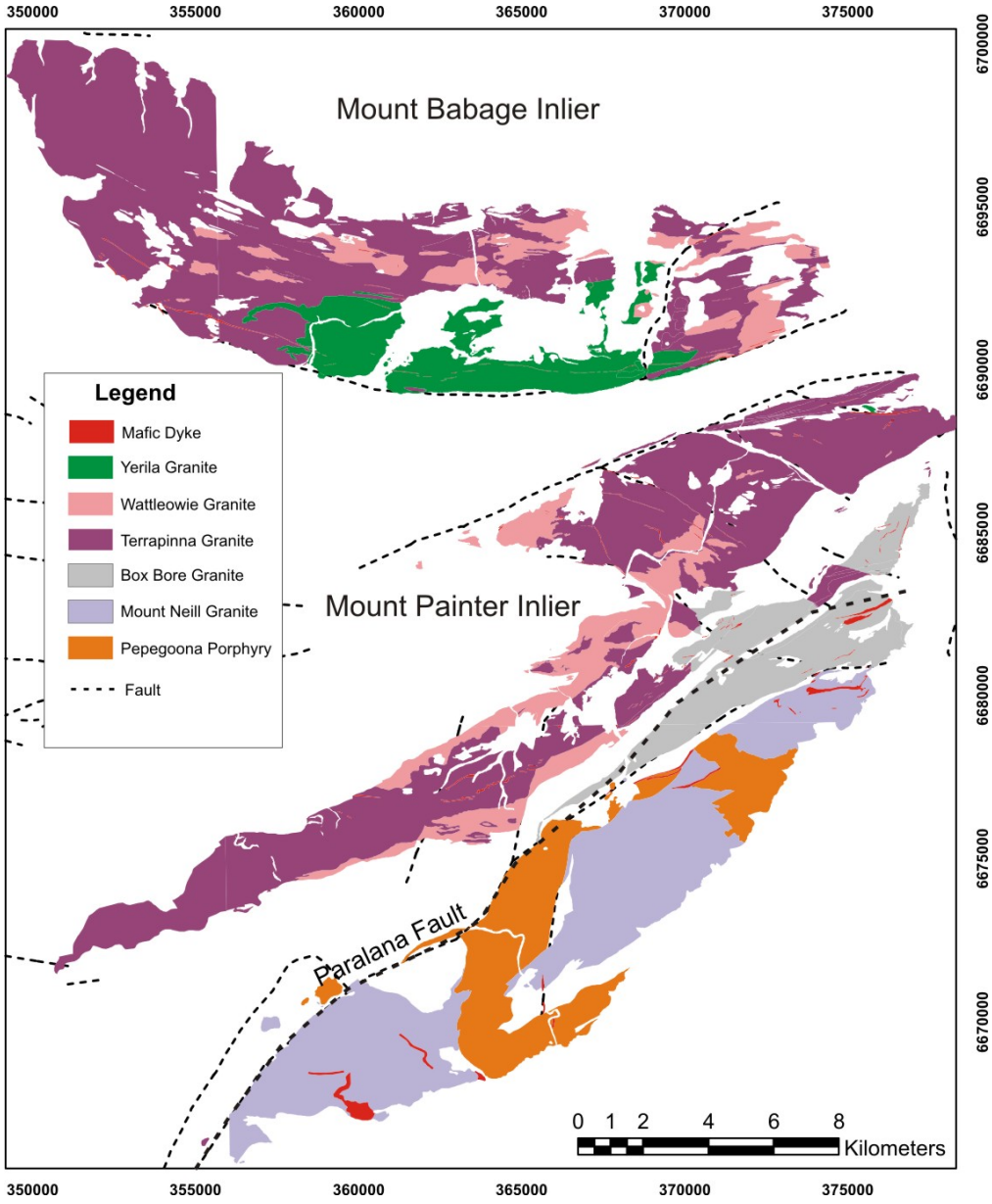

Figure 2.2 Geological map of the Mt Painter Province showing Mesoproterozoic granitic and volcanic rocks.

2.4 Lithology of mafic-felsic magmatic rocks

Mesoproterozic mafic-felsic magmatic rocks of the Mount Painter Province are divided into seven main lithological suites in this studies including; 1) Pepegoona Volcanics, 2) Mt Neill Granite, 3) Box Bore Granite, 4) Terrapinna Granite, 5) Wattleowie Granite, 6) Yerila Granite and associated microgranular enclaves and 7) mafic dykes. This section describes lithological and petrographical characteristics of the magmatic suites based on outcrop, hand specimen samples and thin section descriptions from Mt

Babbage Inlier and northern Mt Painter Inlier. Figure 2.3 shows the granitic and volcanic sample locations in the study area.

2.4.1 Pepegoona Volcanic

The Pepegoona Volcanics are interlayered with metasediments, which are interpreted as shallow-water marine to non-marine clastic sedimentary rocks (Teale, 1993b), and are found in south-east of the Mt Painter Inlier. They are typically massive to blocky in outcrop and conformably overlie the metasediments. The volcanics are intruded by the Mt Neill Granite (Figure 2.4). The boundary between the volcanic and metasedimentary rocks may be difficult to recognise due to shearing during the Delamarian Orogen. A well-developed foliation in the volcanics is typically consistent with lava flow banding. The Pepegoona Volcanics are typically dark grey to red in colour; fine-grained and porphyritic (Figure 2.5a). Pheonocrysts include pink K-feldspar and blue quartz. The K-feldspar phenocrysts are subhedral, tubular to round in shape and strongly altered. Based on their composition, the Pepegoona Volcanics are rhyolite and dacites.

The Pepegoona Volcanic contain 40% rounded to sub-rounded quartz (1-10 mm in size), tabular to sub-rounded plagioclase (2-15 mm in size), strongly to intermediate sericite-altered clinopyroxene (2-10 mm in size) and tabular K-feldspar (2-15 mm in size) phenocrysts and 60% fine-grained quartz and feldspar groundmass. The quartz and feldspar groundmass shows alignment following the outline of phenocrysts suggesting magmatic flow (Figure 2.5b). Ovoid phenocrysts are typically rimmed by finer-grained quartz. Muscovite, chlorite and sericite are found as secondary minerals, and interpreted to have formed as a result of metamorphism and/or alteration.

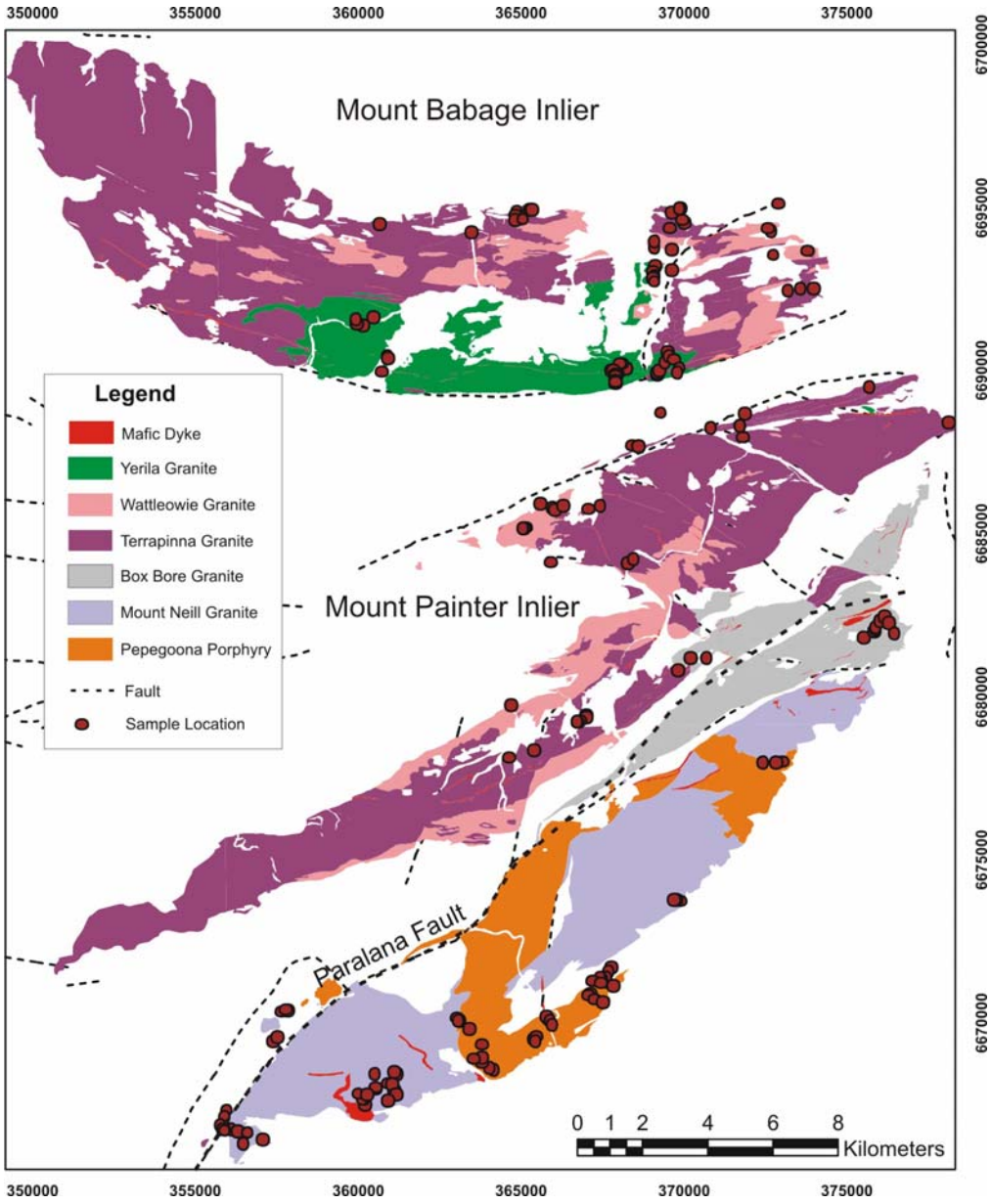

Figure 2.3 Geological Map of Mt Painter Province showing sample locations.

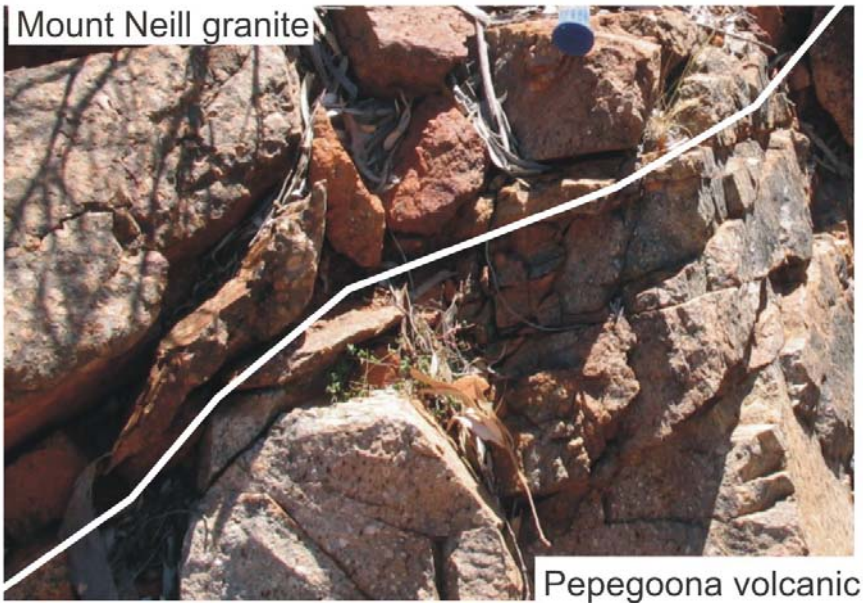

Figure 2.4 Contact between porphyritic Pepegoona volcanic and coarse-grained Mount Neill granite.

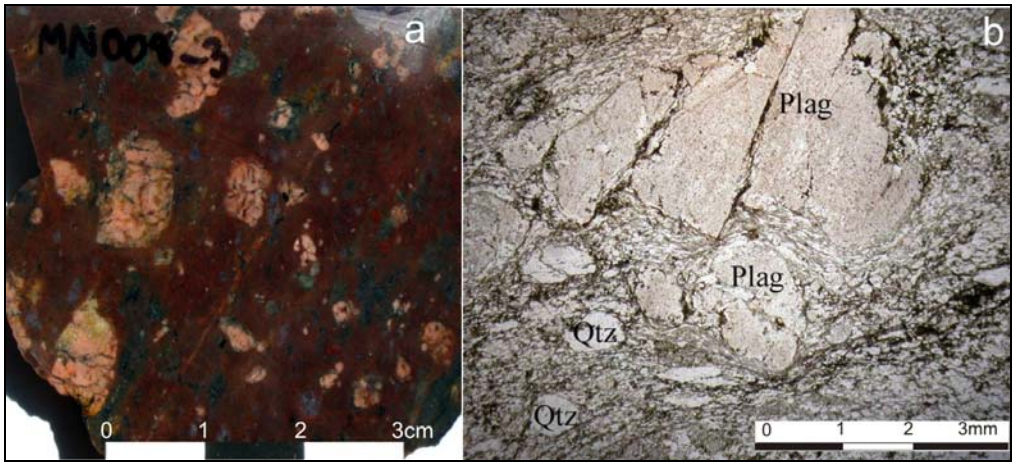

Figure 2.5 Porphyritic Pepegoona volcanics: a) Strongly altered feldspar phenocryst from sample MN008; b) Subrounded plagioclase (Plag) phenocrysts and rounded quartz (Qtz) phenocrysts in groundmass showing magmatic flowing bands from sample MN061 in plane polar.

2.4.2 Mount Neill Granite

The Mt Neill Granite crops out in the south-east, central and north of the Mt Painter Inlier. It has intrusive contacts with the Pepegoona Volcanics. Based on grain size, the Mt Neill Granite can be divided into two groups 1) fine-grained and 2) medium- to coarse-grained (Figure 6a and 6b). The medium- to coarse-grained granites are the dominant group in the study area

and are characterised by equigranular to inequigranular, red- to pink-altered phenocryst and groundmass, with rounded feldspar and blue quartz phenocrysts in a finer quartz, feldspar and biotite groundmass. The phenocrysts are medium to megacrystic in size (up to 5 cm). In thin sections, the medium- to coarse-grained Mount Neill granites typically comprise coarse-grained (phenocryst) and finer grained (groundmass) quartz (40-45%, 0.5-15 mm), fine- to coarse-grained microcline (30-35%, 0.5-15 mm), plagioclase (15-20%, 2-4 mm), albite (5-10%, 2-3 mm) and biotite (10%, 0.5-2 mm). Phenocrystic quartz typically has a rounded shape with sieve texture and sometimes is rimmed by finer quartz grains as a resorption texture (Figure 2.6c). Coarse-grained microcline phenocrysts exhibit sieve texture and are sometimes surrounded by sodic feldspar suggesting a rapakivi texture. K-feldspar crystals are microperthite. Plagioclase phenocrysts show ovoided to lath shapes. Biotite is generally segregated and may be metamorphosed. Zircon, fluorite, magnetite, apatite, allanite, and monazite are found as accessory minerals, and are more abundant in the medium- to coarse-grained Mount Neill granite. Enclaves found in the medium- to coarse-grained Mount Neill granite consist of 60% quartz and 40% clinopyroxene (Figure 2.6d). The fine-grained granite that is massive, equigranular and red to pink in colour comprise quartz, feldspar and biotite. Mafic enclaves are rarely found. The fine-grained Mt Neill Granite is typically equigranular and subhedral to anhedral and consists of quartz (35-40%, 0.5-4 mm), microcline (30-35%, 0.5-2 mm), clinopyroxene, (15%, 0.5-2 mm), perthite (5-10%, 1-2 mm), plagioclase (5%, 2 mm) and biotite (3%, 0.5-1 mm). Quartz crystals sometimes show shadow extinction resulting from deformation and metamorphism and show granophyric texture (intergrowth of quartz and K-felspar). Feldspars, amphibole and clinoproxene are generally replaced by clay minerals and sericite. Muscovite is interpreted to have formed from the metamorphism of biotite.

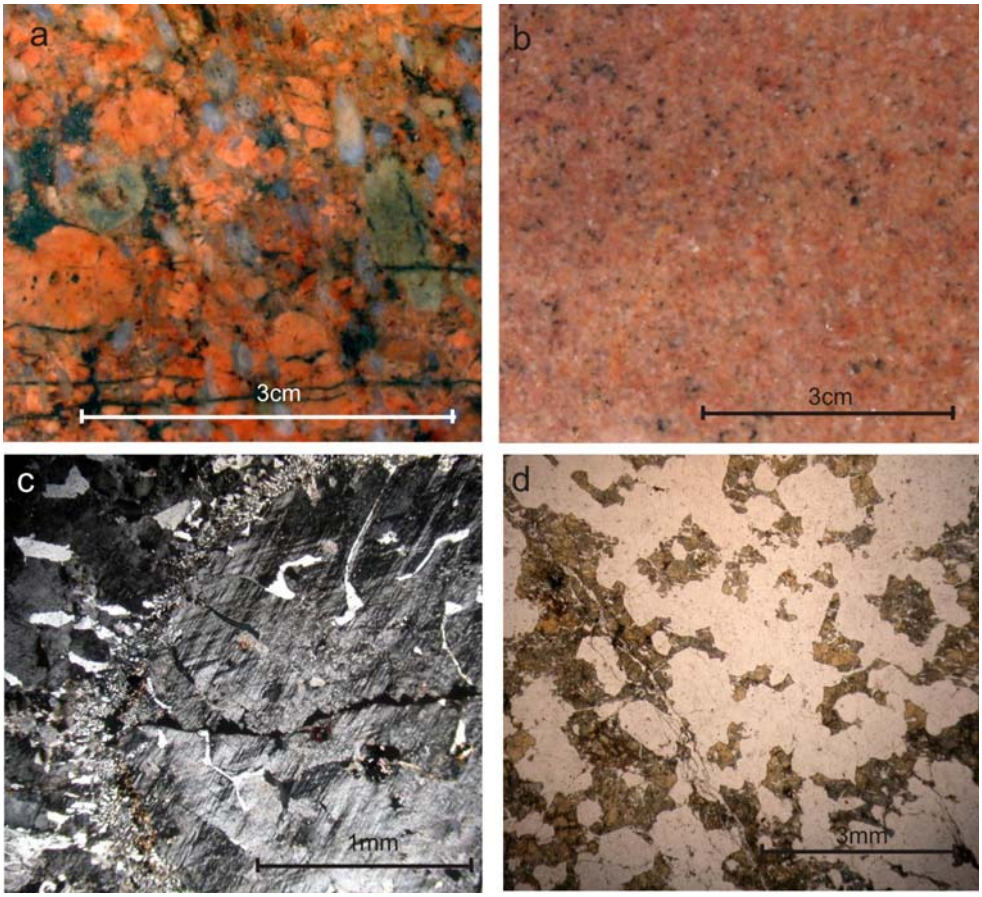

Figure 2.6 Mount Neill granite: a) Strongly altered K-feldspar phenocryst from sample MN067; b) fine-grained equigranular granite from sample MN026; c) fine-grained quartz surround rounded K-felspar phenocryst; d) quartz, amphibole and clinopyroxene from xenolith within Mount Neill granite.

2.4.3 Box Bore Granite

The Box Bore Granite is strongly deformed showing augen quartz and feldspar, and a gneissic texture (Figure 2.7a). It crops out in the north-eastern Mt Painter Inlier and is separated from the Mt Neill Granite by the Paralana fault zone and a mafic dyke. The granite is typically pink to red with altered round coarse-grained (up to 5 cm) K-feldspar.

The Box Bore granite is typically characterised by an inequigranular and porphyritic texture. A gneissic texture is also common. The granite consists of quartz (40%, 5-50 mm), microcline (35%, 2-50 mm), biotite (10%, 1-3 mm) and plagioclase (5%, 1-4 mm). Phenocrystic microcline contains microphertite, quartz and plagioclase grains and is rimmed by fine grained quartz (Figure 7b). Quartz has recrystallised and shows an extinction shadow.

Plagioclase normally is strongly altered to sericite. Zircon, allanite, sphene, apatite and fluorite are abundant in this granite.

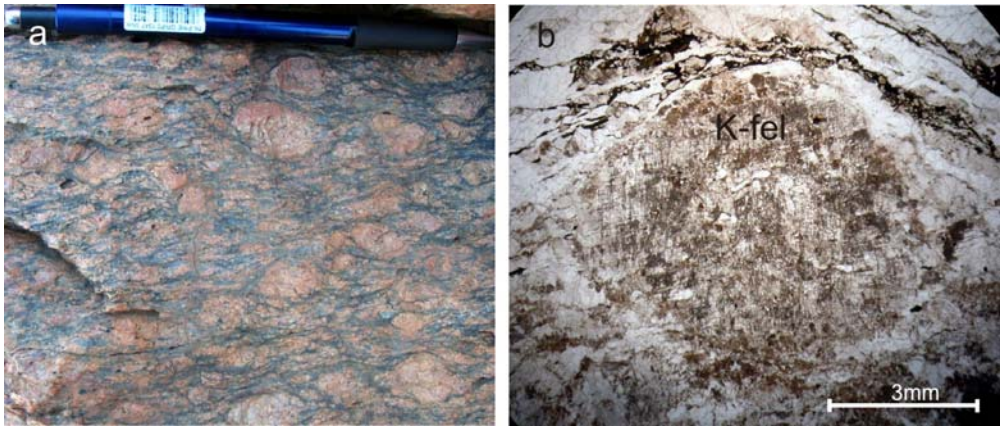

Figure 2.7 Box Bore granite; a) altered and foliated porphyritic Box Bore granite outcrop from the East of Mt Painter Inlier; b) coarse-grained ovoidal K-feldspar phenocryst in the Box Bore granite.

2.4.4 Terrapinna Granite

The Terrapinna Granite has the largest area of outcrop in the study area and occurs in both the Mt Painter and the Mt Babbage inliers. It is typically medium- to coarse-grained, white to pale grey and porphyritic, with ovoidal feldspar and quartz megacrysts (up to 15 cm) and biotite (Figure 2.8a). The granite has a strongly gneissic texture. The Terrapinna Granite is intruded by the Wattleowie Granite.

The Terrapinna Granite is petrographically characterised by inequigranular to equigranular, anhedral, medium- to coarsed-grained and slightly to strongly metamorphosed with a gneissic texture. It comprises feldspar (40%, 2-50 mm of K-feldspar; 20%, 5-30 mm of plagioclase), quartz (25%, 0.5-15 mm) and biotite (7%, 1-5 mm). Megacrystic ovoid K-feldspars show perthitic and albitic replacements, fine-grained quartz rim and a granophyric texture (Figure 2.8b). Plagioclase which is intensively replaced by sericite is found as overgrowths on K-feldspar megacrysts. Biotite laths may show kink bands as a result of metamorphism and deformation, and may contain zircon inclusions.

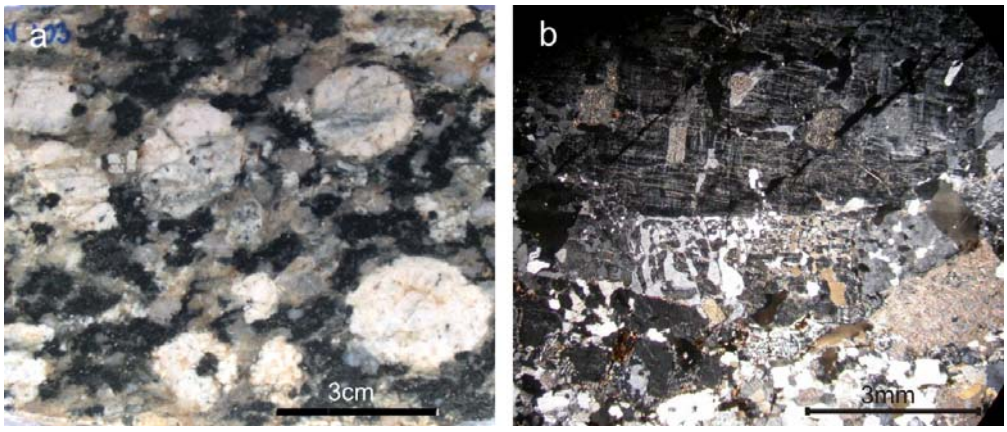

Figure 2.8 Terrapinna Granite; a) coarse-grained, rounded K-feldspar phenocryst from sample MN103; b) fine-grained quartz rim-granophyric texture.

2.4.5 Wattleowie Granite

The Wattleowie Granite crops out in the northern the Mt Babbage Inlier and central Mt Painter Inlier and is intruded by Mudnawatana tonalites. It is spatially associated with the Terrapinna Granite with which it has a gradational contact at some localities. The granite is typically white to pale grey, equigranular, weakly deformed with a spotted appearance (Figure 2.9a and 2.9b). In hand-specimen, its mineralogy consists of quartz, feldspar and biotite.

The Wattleowie Granite is typically fine-grained and equigranular. It consists of quartz (45%, 0.1-1 mm), microcline (25%, 1-3 mm), perthitic K-feldspar (17%, 2-12 mm), and biotite (10%, 0.5-3 mm). This granite is affected by metamorphism and/or alteration, showing a sieving texture, extinction shadow in quartz and secondary minerals such as muscovite, sericite and chlorite. Zircon is found in biotite, showing a radioactive halo. Apatite and fluorite are accessory minerals.

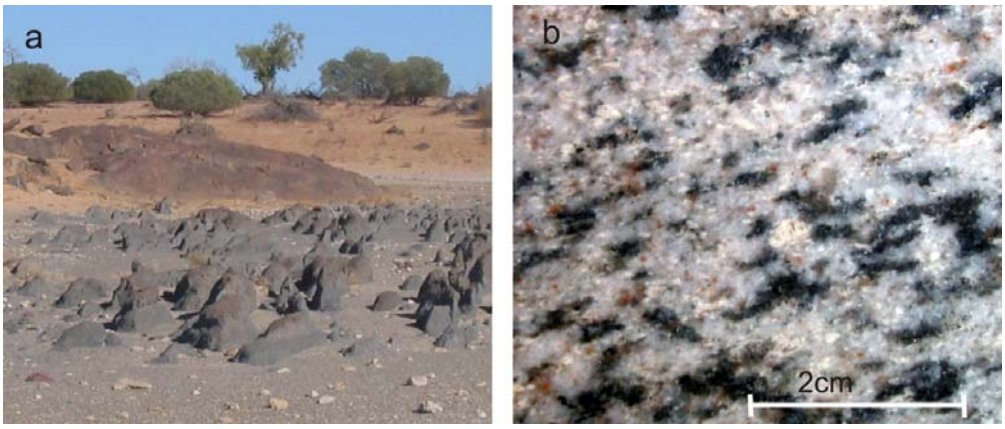

Figure 2.9 Wattleowie granite; a) Field outcrop characterise of the Wattleowie granite at the north of the Mt Babbage Inlier; b) fine-grained equigranular Wattleowie granite.

2.4.6 Yerila granite and microgranular enclaves

The Yerila Granite is located in the southern Mt Babbage Inlier and is typically deformed. It is characteristically pale grey, medium- to coarse-grained and inequigranular. In hand specimen, its mineralogy consists of tabular feldspar, quartz and feldspar. Yellow allanite grains may also be seen in hand specimen. The Yerila Granite commonly contains mafic and felsic enclaves (Figure 2.10a and 2.10b). Enclaves are sub-rounded to sub-angular with minor irregular or fusion-form shapes and contact boundaries are sharp to diffuse and may show fine-grained darker rims of ferromagnesian minerals. Pegmatite and mafic dykes have a crosscutting relationship with the Yerila Granite.

In thin section, the Yerila Granite is typically medium-grained, euhedral to anhedral and inequigranular comprise phenocrysts of tabular microcline (25%, 10-50 mm) and tabular plagioclase (15%, 10-30 mm) and groundmass of quartz (40%), microcline (10%) and biotite (10%; Figure 10c). Quartz is recrystallised and deformed showing fine-grained aggregates and extinction shadows. Accessory minerals including zircon, apatite, allanite, fluorite, sphene and magnetite are abundant in Yerila granite (up to 3%).

Allanite is generally found with biotite and is 3-5 mm in size. Mafic enclaves are fine- to medium grained, and consist of 35% biotite (0.5-3 mm), 25% hornblende (1-5 mm), 15% plagioclase (1-3 mm), 10% K-feldspar (2-30 mm), 7% quartz (1-6 mm) and 3% allanite (Figure 2.10d). Phenocrystic K-

feldspar in mafic enclaves has the same morphology as K-felspar phenocrysts in the host Yerila granite. Accessory minerals are extremely enriched (up to 5%) in the mafic enclaves including allanite (yellow to orange, subhedral to euhedral, zoning, and altered, 2-10 mm; Figure 2.7d), sphene (colourless, subhedral to anhedral, 0.2-1 mm), apatite (euhedral, 0.1-0.3 mm), zircon (euhrdral, 0.1-1 mm), fluorite (anhedral, 0.1-10 mm) and unidentified U-Th minerals.

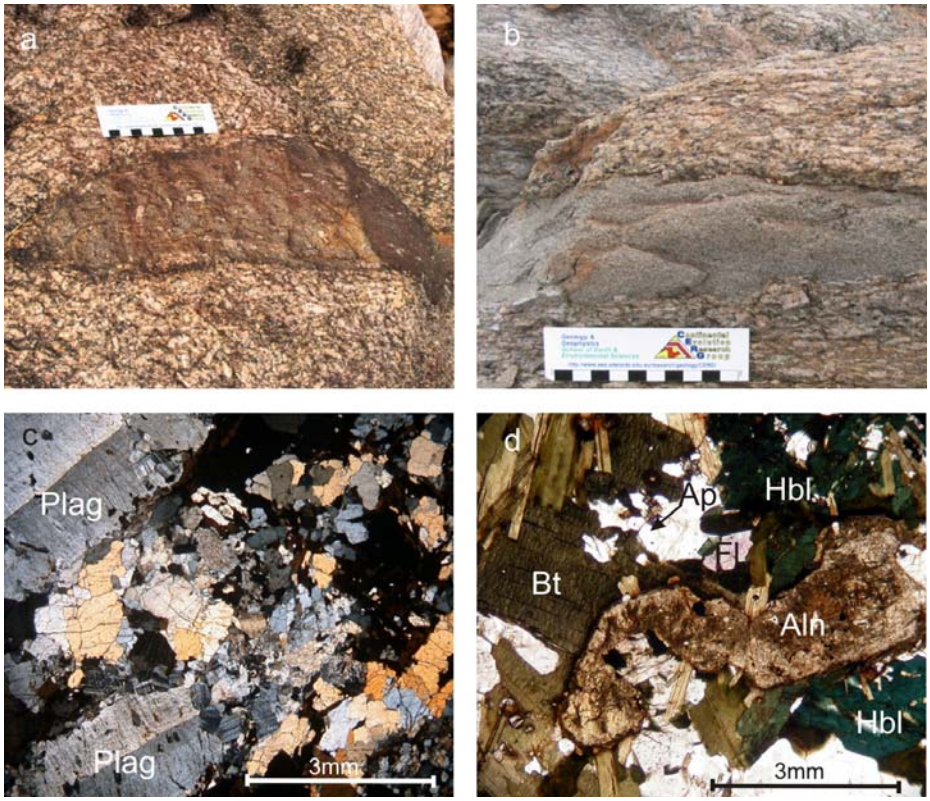

Figure 2.10 The Yerila granite and Microgranular enclaves; a) outcrop mafic microgranular enclave within Yerila granite containing tabular feldspar phenocryst; b) outcrop felsic microgranular enclave within Yerila granite; c) plagioclase phenocryst within quartz-k-feldspar-plagioclase-biotite groundmass; d) subeuhedral allanite crystal (Aln), hornblende (Hbl), biotite (Bt), apatite (Ap) and fluorite (Fl) in microgranular enclave.

2.4.7 Mafic dyke

Mafic dykes are oriented NW-SE and NE-SW. They intrude into volcanic, granitic and metasedimentary rocks as sills and dykes (Figure 2.11a and 2.11b). The largest dykes are approximately 50 m wide and 2-3 km long. There are at least two generations of mafic dykes; the first have been strongly deformed and the second which are undeformed.

Mafic dykes of the study area are generally dark grey, fine-grained and equigranular. Plagioclase and hornblende can be observed in hand specimens, and they are altered to differing degrees.

Mafic dykes are mainly mafic to intermediate. Basaltic (doleritic) dykes are typically fine-grained and equigranular, and consists of 40% anhedral cluster to euhedral acicular amphibole (0.1-3 mm), 40% plagioclase (0.2-1 mm), 7% biotite, 5-7% opaque minerals (ilmenite and magnetite) and 3% quartz (Figure 2.11c). Apatite, zircon and allanite are accessory minerals. Andesite dykes comprise amphibole (35%, 0.2-2 mm), biotite (25%, 0.1-1 mm), quartz (20%, 0.1-0.3 mm), plagioclase (10%, 0.5-1 mm), clinopyroxene (5%) and opaque minerals (Figure 2.11d). Zircon and apatite are abundant, occurring as inclusion in amphibole and biotite. Allanite and titanite are also found as accessory minerals. Metamorphic garnet is found in a Mount Babbage andesitic dyke.

The strongly deformed mafic dykes that are coeval to the HHP granites (see Chapter 4) are grouped as Mesoproterozoic mafic dykes. The undeformed mafic dykes that have low heat production values (see Chapter 5) are grouped as Paleozoic mafic dykes. Based on geochronological data (see Chapter 4), Neoproterozic mafic dykes are also found in the Mt Painter Province. Therefore, the mafic dykes in this study are divided into three groups including Paleozoic, Neoproterozoic and Mesoproterozoic mafic dykes.

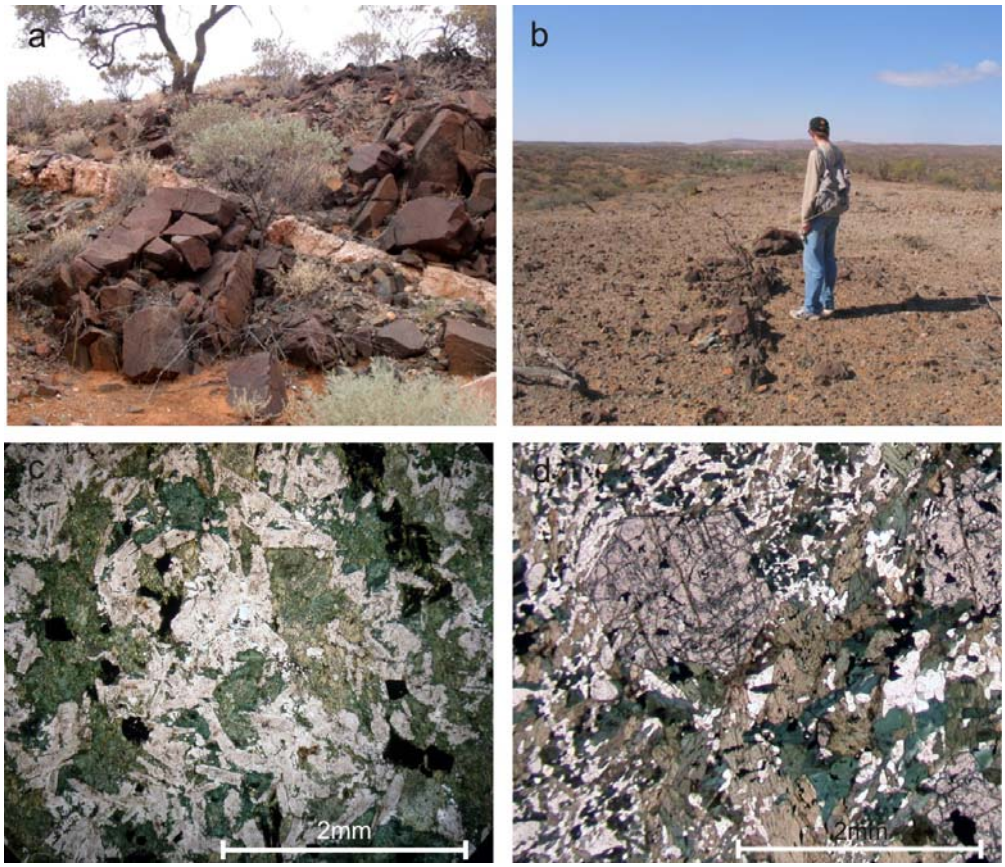

Figure 2.11 Mafic dyke; a) An outcrop of mafic dyke and pegmatitic dyke cross-cutting the Yerila granite in the south of the the Mt Babbage Inlier; b) mafic dyke cross-cutting the Yerila granite in the centre of the Mt Babbage Inlier; c) A photomicrograph of amphibole, plagioclase, biotite, ilmenite and magnetite in a mafic dyke (Sample MN090); d) A photomicrograph of garnet, hornblende, biotite and quartz in a mafic dyke (Sample BB06).

Chapter 3 Mineralogy

This chapter describes the mineralogy of the granites and associated rocks of the Mt Painter Province. These include feldspar, biotite, amphibole, zircon, allanite, apatite, Ti-minerals and U-Th minerals. Mineral compositions were determined using an electron microprobe for major elements and by LA-ICPMS for trace elements. The methodology is given in Appendix 3.

3.1 Major minerals

3.1.1 Feldspar

Feldspars are found in all rock types in this study. Both plagioclase and K-feldsapr are typically found in the felsic igneous rocks and microgranular enclaves, whereas plagioclase is only feldspar found in the mafic dykes.

The porphyritic Pepegoona Volcanics contain both plagioclase and K-feldspar as phenocrysts and groundmass. Feldspar phenocrysts are 0.2 to 10 mm in size, subequant to ovoid in shape and partly replaced by sericite and chlorite. Twinning and oscillatory zoning are rarely preserved in K-feldspar phenocrysts.

Feldspars from Mt Neill and Box Bore Granites are fine- to coarse-grained (1 to 15 mm), anhedral to subhedral with tabular to rounded shapes. The coarse ovoid feldspars show resorption rims. Sericitic alteration is commonly found in Mt Neill feldspars. The Terrapinna Granite typically contains medium to megacrystic (2 cm long on average, but up to 10 cm long) K-feldspar and plagioclase. The megacrystic feldspars are typically rounded showing quartz-overgrowths. Sericite-altered plagioclase crystals are also found. These could suggest recrystallization of the feldspars.

In the Wattleowie Granite, K-felspar and plagioclase are generally anhedral to euhrdral, fine- grained (1-3 mm) and show zoning. Feldspar grains contain muscovite and fine-grained quartz.

Feldspars from the Yerila Granite include plagioclase and K-feldspar, occurring as phenocrysts and groundmass. The phenocrysts are mainly tabular euhedral K-feldspar. The groundmass is finer grained K-feldspar, quartz and

biotite. Microgranular enclaves contain K-feldspar phenocryst with the same characteristics as the host Yerila Granite. Feldspar in mafic dykes is typically equigranular, fine-grained and tabular plagioclase.

The Pepegoona Volcanic and the Mt Neill, Box Bore, Wattleowie and Terrapinna Granites contains plagioclase, which is orthoclase and high albite (An_{1-67}), and K-feldspar, which is microcline and perthite (Or_{76-97}; Table 3.1; Figure 3.1). The Yerila Granite has plagioclase, which is andesine and oligoclase (An_{29-32}), and K-felpar, which is microcline (Or_{91-95}; Figure 3.2). Plagioclase of mafic microgranular enclaves has a range of composition from oligoclase to andesine (An_{11-32}), whereas Plagioclase of felsic microgranular enclaves has a range of composition anothoclase, oligoclase and andesine (An_{10-69}). K-feldspr from the mafic and felsic enclaves is microcline (Or_{94-96}). Mafic dykes (Mesoproterozoic and Neoproterozoic mafic dykes) contain plagioclase, which is oligoclase, andesine and labradorite A(n_{13-63}; Figure 3.3).

Plots of Na versus Ca in feldspar display two variation trends including a Major Series and Minor Series suggest different cationic substitution (Figure 3.4). The Major Series, which includes plagioclase from all rock units, has higher Na and Ca content than the Minor Series, which include mainly plagioclase from microgranular enclaves. The ionic variation in the Major Series suggest continuous albite substitute summarised as $Ca^{2+} + Al^{3+} <=> Na^{+} + Si^{4+}$ (Bowen, 1915). Palgioclase from the Minor Series reflects cation deficieny in the Z-site and high Si in the X-site, which may due to entry of Si or Al into the Z-site of a disordered crystal structure (Deer et al., 1992).

Table 3.1 Selected feldspar analyses to represent the different unit of granitic and volcanic rock from the Mt Painter Province.

Sample	MN092	MN092	MN096	MN096	SD047	SD047	MN02	BB021	MN061	BB025	BB018	BB18	HPG05	HPG05	SD010	SD010	MN090	SD004	MN099
Unit	YG	YG	MME	MME	FME	FME	MN	MN	PV	PV	WT	WT	TP	TP	BB	BB	MMF	NMF	PMF
SiO2	63.38	56.53	62.72	60.52	62.65	62.28	62.81	64.99	64.13	63.43	62.74	64.38	63.59	66.23	64.61	65.53	59.19	58.51	55.78
Al2O3	18.04	22.93	17.24	23.68	17.74	22.73	17.66	22.38	17.98	22.15	17.48	21.19	17.93	20.70	18.00	20.88	25.68	25.65	27.28
FeO	0.03	0.01	0.36	0.41	0.08	0.33	0.02	0.00	0.03	0.09	0.00	0.00	0.04	0.08	0.10	0.07	0.23	0.05	0.01
CaO	0.00	6.22	0.00	6.03	0.00	4.12	0.00	3.37	0.01	3.72	0.01	2.91	0.06	0.72	0.00	1.67	7.54	7.82	9.60
Na2O	0.71	7.51	0.50	8.24	0.44	6.66	0.67	8.76	0.47	9.57	0.35	9.71	0.41	9.39	0.53	9.45	7.47	7.31	5.89
K2O	16.34	0.19	14.68	0.16	16.76	2.34	16.34	0.11	16.57	0.14	16.48	0.12	16.41	0.41	16.45	0.09	0.05	0.09	0.05
BaO	0.29	0.00	0.14	0.00	0.11	0.08	0.00	0.00	0.04	0.00	0.52	0.00	0.13	0.00	0.15	0.06	0.00	0.00	0.00
Toatal	98.81	93.39	95.70	99.10	97.83	98.68	97.59	99.66	99.26	99.20	97.65	98.49	98.71	97.60	100.00	97.79	100.16	99.56	98.61
Cations based on 32 oxygens																			
Si	12.221	10.899	12.094	11.668	12.080	12.009	12.111	12.531	12.366	12.231	12.097	12.413	12.261	12.769	12.457	12.635	11.412	11.282	10.755
Al	4.099	5.210	3.918	5.380	4.032	5.166	4.013	5.086	4.086	5.033	3.973	4.816	4.074	4.703	4.090	4.744	5.835	5.828	6.198
Fe(ii)	0.004	0.001	0.058	0.066	0.013	0.053	0.003	0.000	0.004	0.015	0.000	0.000	0.006	0.013	0.017	0.011	0.037	0.008	0.001
Ca	0.000	1.284	0.000	1.246	0.000	0.851	0.000	0.696	0.003	0.769	0.002	0.602	0.012	0.148	0.000	0.344	1.557	1.614	1.982
Na	0.264	2.808	0.187	3.079	0.164	2.489	0.252	3.275	0.174	3.577	0.133	3.631	0.153	3.511	0.199	3.533	2.792	2.734	2.202
K	4.019	0.046	3.609	0.040	4.122	0.576	4.020	0.026	4.074	0.034	4.052	0.029	4.036	0.101	4.046	0.022	0.013	0.023	0.012
Ba	0.022	0.000	0.011	0.000	0.008	0.006	0.000	0.000	0.003	0.000	0.039	0.000	0.009	0.000	0.011	0.005	0.000	0.000	0.000
TOTAL	20.629	20.248	19.877	21.479	20.419	21.150	20.400	21.615	20.710	21.659	20.295	21.491	20.553	21.246	20.821	21.294	21.647	21.489	21.150
Ab	6.17	67.86	4.93	70.53	3.82	63.56	5.90	81.93	4.09	81.67	3.17	85.19	3.64	93.36	4.68	90.61	64.00	62.54	52.48
An	0.00	31.04	0.00	28.55	0.00	21.72	0.00	17.42	0.07	17.56	0.04	14.12	0.29	3.95	0.00	8.83	35.69	36.93	47.24
Or	93.83	1.10	95.07	0.92	96.18	14.71	94.09	0.66	95.83	0.77	96.79	0.69	96.07	2.69	95.32	0.56	0.31	0.53	0.28

YG: Yerila Granite, MME: Mafic microgranular enclave, FME: Felsic microgranular enclave, MN: Mount Neill Granite, PV: Pepegoona Volcanic, WT: Wattleowie Granite, TP: Terrapinna Granite, BB: Box Bore Granite, MMF: Mesoproterozic mafic dyke, NMF: Neoproterozoic mafic dyke, PMF: Palaeozoic mafic dyke.

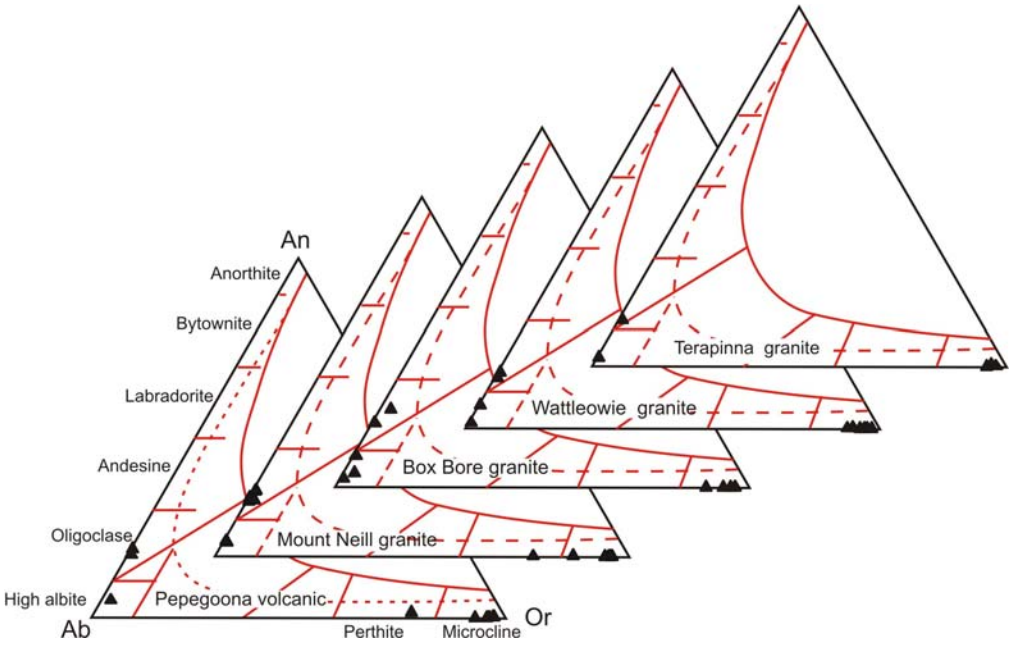

Figure 3.1 Variations of feldspar compositions from volcanic and granitic rocks of the Mount Painter Province.

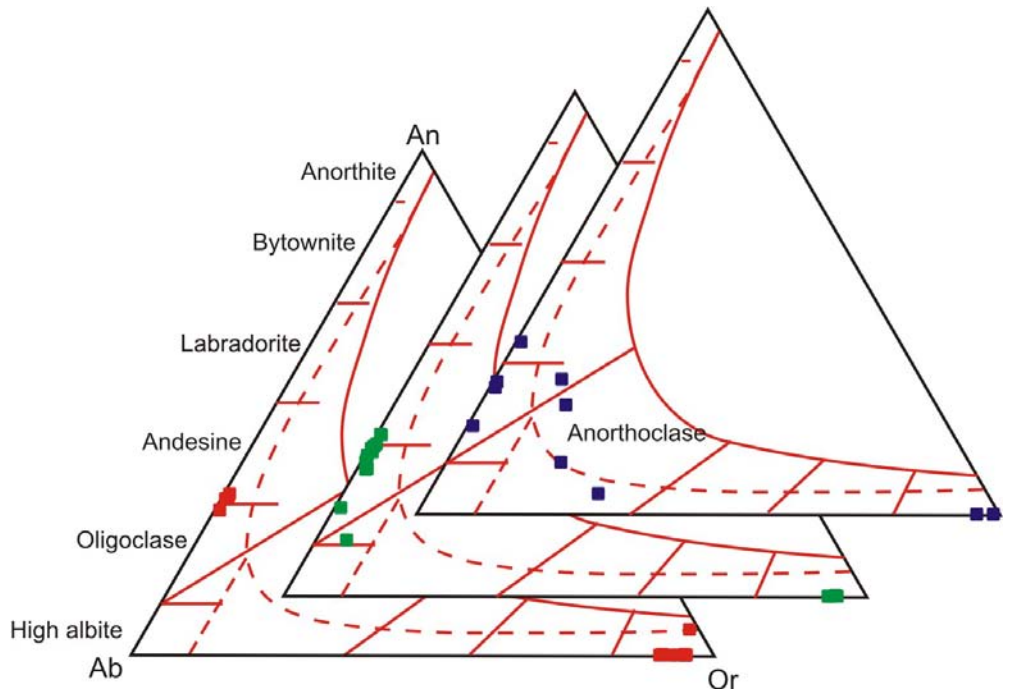

Figure 3.2 Variations of feldspar compositions from the Yerila granite and associated microgranular enclaves (Symbols; Red: Yerila Granite feldspar, Green: Mafic microgranular enclave, Blue: Felsic microgranular enclave).

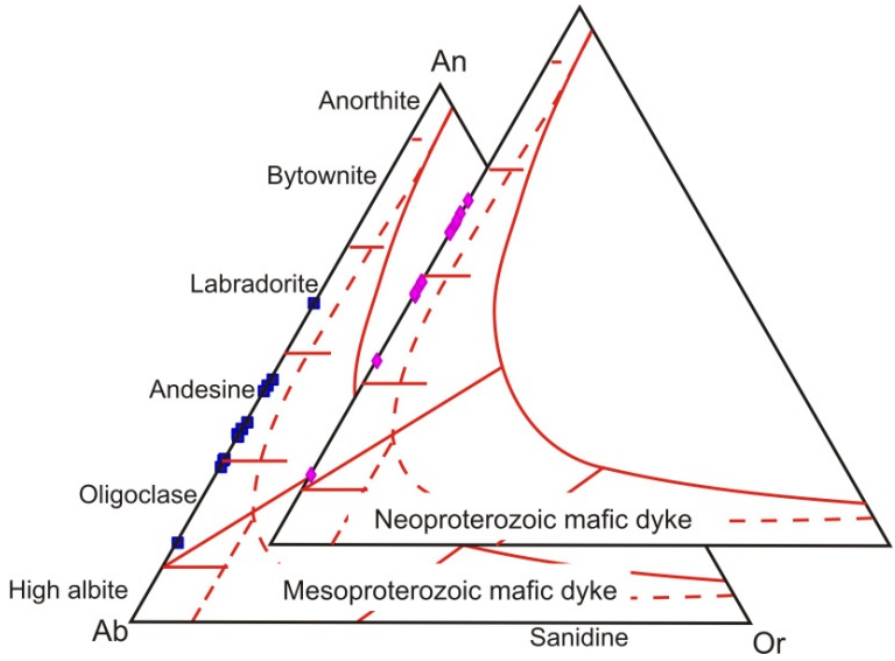

Figure 3.3 Variations of plagioclase feldspar compositions of mafic dykes from Mount Painter Province.

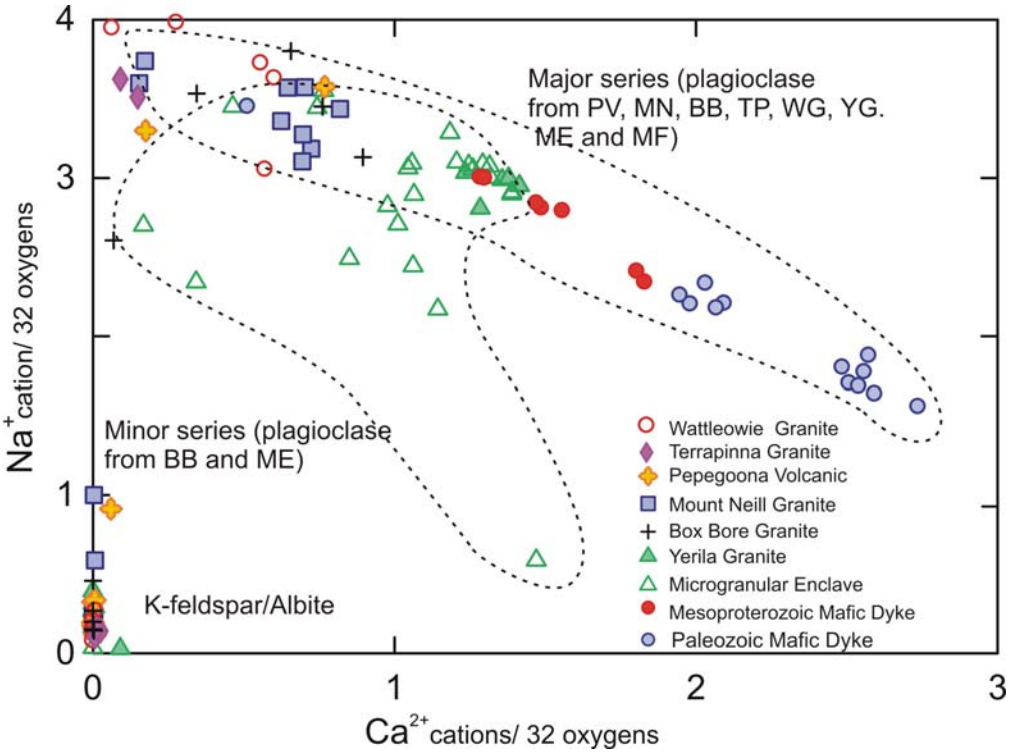

Figure 3.4Variations of Na+ versus Ca2+ in feldspars of mafic and felsic igneous rocks from the Mt Painter Province showing two trends that suggest differing cationic substitution (PV: Pepegoona volcanic, MN: Mt Neill granite, BB: Box Bore Granite; TP: Terrapinna Granite, WG: Wattleowie Granite, YG: Yerila Granite, ME: microgranular enclave, MF: mafic dyke).

Feldspars from this study were plotted with the geothermometer based on ternary feldspar compositions after Deer et al. (1992: Figure 3.5) Most feldspars plot in the 700 °C field, however feldspars from felsic microgranular enclaves plot in a higher temperature field (800-900 °C) and one feldspar analysis from the Yerila Granite suggests a temperature of formation of approximately 900°C.

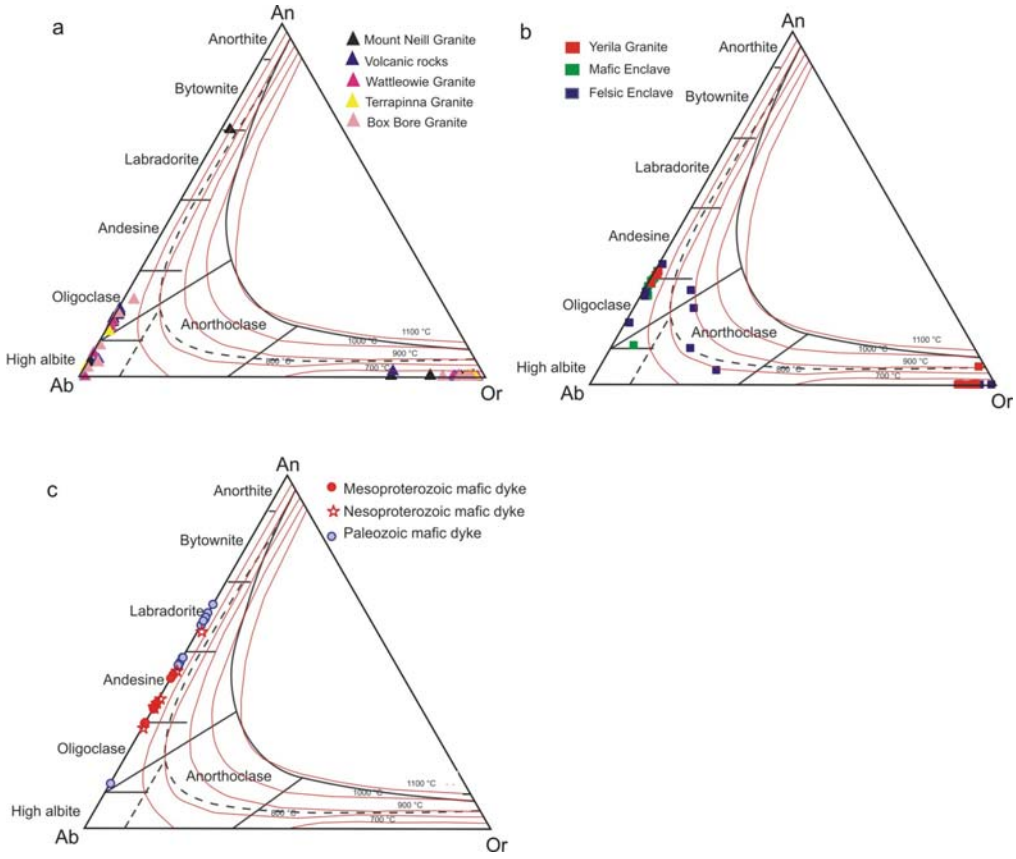

Figure 3.5 Geothermometer of ternary feldspar compositions for mafic and felsic igneous rocks from Mount Painter Province (after Deer et al., 1992).

Trace elements in feldspars from most rock units using LA-ICPMS are lower than detection limits, except from the Yerila Granite and microgranular enclaves. Feldspars from the Yerila Granite and microgranular enclaves have low LREE contents and low to very low HREE, Y, Th and U contents. Chondrite-normalized REE patterns generally show enriched LREE, flatter HREE and positive Eu anomalies (Figure 3.6). REE contents in feldspars from microgranular enclaves are relatively higher than feldspar from the Yerila granite. The positive Eu anomaly of the feldspar suggests that the feldspar disequilibrium occurs by trace-element undersatuaration which is

ascribed to slow dissolution rates of accessory phases in water-poor melts (Carrington and Watt, 1995).

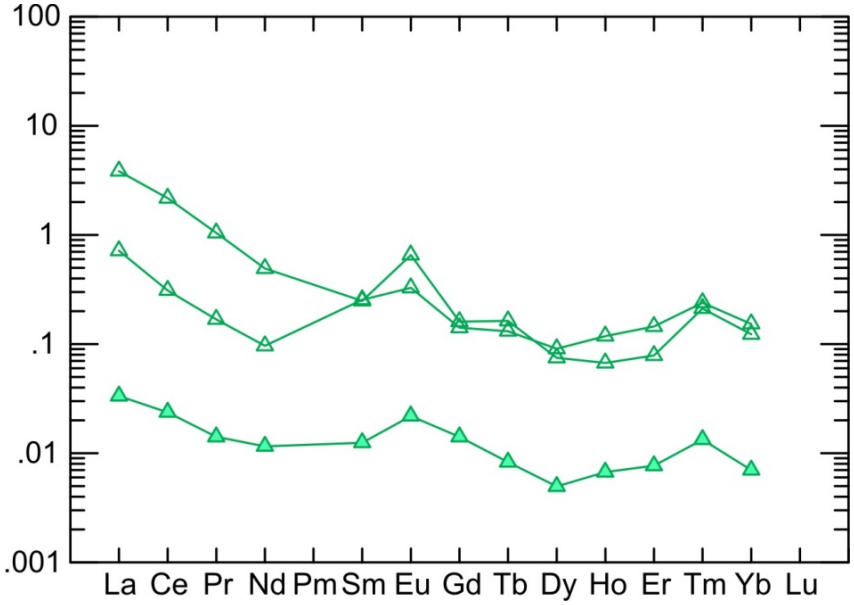

Figure 3.6 Rare earth element concentrations normalised to chondrite values (Sun and McDonald, 1989) of feldspar from Yerila granite and microgranular enclave (Symbol; closed triangular: Yerila granite and opened triangular: microgranula enclave)

The absence of simple twinning, oscillatory zoning, euhedral inclusions of plagioclase and crystallographically controlled arrangements of inclusions, which indicate igneous K-feldspar (e.g. Vernon, 1986; Vernon, 1999), suggest that the K-feldspar from all units in this study has been affected by metamorphism. K-Feldspar megacrysts are interpreted to have grown at a late stage, during cooling of the granitic magma in subsolidus conditions (Vernon, 1986), so they formed by textural coarsening after the groundmass crystallized at subsolidus temperatures (Johnson et al., 2006). K-feldspar megacrysts have been suggested to form as a result of magma mixing in granitic rocks (e.g. Vernon, 1990; Gagnevin et al., 2004; Collins et al., 2006). K-feldspar phenocrysts from microgranular enclaves derived from disintergration replenishment dykes of more mafic magma are indented by K-feldspar phenocryst of the Yerila Granite, indicating the K-feldspar were present before the microgranular enclave and the host granites solidified. Alignment of K-feldspar phenocrysts in microgranular enclave and host Yerila Granite interpreted to be a magmatic flow foliation implies that the K-feldspar moved as independent crystals in liquid.

3.1.2 Amphibole

Amphiboles are important mafic minerals because their variable composition can record the chemical evolution of melt during their crystallization and can yield information of magmatic evolution and differentiation (e.g. Gualda and Vlach, 2007). Amphiboles in this study are mainly found in mafic dykes and microgranular enclaves, where they are petrographically and chemically different in each rock units. Amphiboles in mafic dyke occur as tabular crystals and clumps of crystals together with biotite and plagioclase and display pine green to brown pleochroism and often display radioactive damage haloes. Amphiboles in the microgranular enclaves are commonly pleochroic, green, tabular crystals and normally contain zircon, apatite and U-Th minerals as mineral inclusions.

Amphiboles in all samples have calcic compositions (B_{Na} <0.5; Figure 3.7) but show variable chemistry. Amphiboles from microgranular enclaves are nearly homogeneous and are enriched in FeO, MnO, and K_2O and depleted in MgO and Mg/(Mg+Fe^{2+}; Table 3.2). The amphiboles in the microgranular enclave are mainly classified as potassian hastingsite with only one analysis suggesting potassium ferro-pargasitic hornblende (Appendix 3) using the excel spreadsheet developed by A.G. Tindle and P.C. Webb of the Open University (www.open.ac.uk/earth-research/tindle/AGTWebPages/AGT Soft. html), which is calculated based on studies of Leake, (1978), Rock and Leake, (1984) and Mogessie et al., (1990). The alternative classification of Leake et al. (2003) amphiboles in the enclave are mainly Hastingsite (Al^{VI}≤Fe^{3+}) with one analysis showing ferropargasite (Al^{VI}≥Fe^{3+}; Figure 3.8).

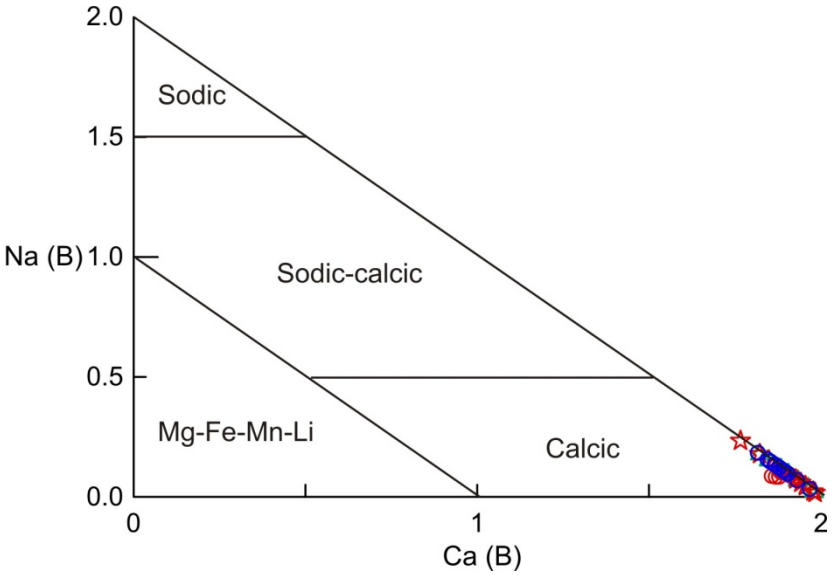

Figure 3.7 Amphibole classifications (B_{Na} versus B_{Ca}) of magmatic-amphibole from mafic dykes and microgranular enclaves showing calcic composition.

Amphiboles from Mesoproterozoic mafic dykes commonly have widely varying major element contents but are depleted in K_2O and Ti_2O. They show variation in amphibole types. The main classifications are actinolitic hornblende and magnesio-hornblende with minor of actinolite, tschermakite, ferrian-tschermakitic hornblende, subsilicic ferro-tschermakite and alumino- tschermakite (Appendix 3). Mesoproterozoic mafic dyke amphiboles are mainly classified as edenite with minor pargasite and magnesiohastingsite (Figure 3.8: Leake et al. (2003). Amphiboles from Neoproterozic mafic dykes commonly have high Na_2O, and low MgO and TiO_2 contents. They are mainly classified as ferro-tschermakite with some analyses showing ferro-tschermakitic hornblende, ferroan pargasite and anthophyllite (Appendix 3); whereas Figure 3.8 displays the amphibole classification after Leake et al. (2003) showing ferropargasite and hastingsite types. Amphiboles of Palaeozoic mafic dykes are typically homogeneous, contain high TiO_2 and are consistently classified as magnesio-hornblende. The classification of Leake et al. (2003) suggests that they are edenite (Figure 3.8).

Table 3.2 Selected amphibole analyses to represent the different unit of granitic and volcanic rock from the Mt Painter Province.

Sample	MN096	MN096	SD051	SD051	MN090	MN090	MN099	MN099
Unit	ME	ME	NMF	NMF	MMF	MMF	PMF	PMF
Spot	Mn96_03	Mn96_04	Sd51_05	Sd51_08	Mn91_02	Mn91_10	Mn91_32	Mn91_35
SiO2	36.76	36.08	39.65	39.35	43.62	44.018	48.19	46.73
TiO2	0.53	0.53	0.32	0.41	0.42	0.401	0.61	0.80
Al2O3	12.22	12.42	14.44	11.90	10.63	10.713	7.62	8.54
FeO	28.62	28.28	21.12	22.27	18.32	17.141	15.80	15.83
MnO	0.58	0.53	0.42	0.40	0.39	0.306	0.28	0.19
MgO	2.22	2.32	6.02	6.67	9.33	9.792	11.76	10.67
CaO	11.00	10.44	11.70	10.47	11.80	11.958	11.96	12.03
Na2O	1.14	1.04	1.40	1.16	1.10	1.095	0.70	0.72
K2O	2.00	2.04	0.42	0.60	0.28	0.223	0.35	0.39
BaO	0.00	0.00	0.05	0.00	0.00	0.075	0.00	0.02
Structural formulae based on 23 oxygens								
Si	6.027	5.962	6.145	6.194	6.591	6.643	7.069	7.007
Al iv	1.973	2.038	1.855	1.806	1.409	1.357	0.931	0.993
Al vi	0.388	0.380	0.781	0.402	0.485	0.549	0.387	0.515
Ti	0.065	0.066	0.037	0.048	0.048	0.045	0.067	0.090
Fe3+	0.808	1.066	0.605	1.301	0.627	0.478	0.386	0.144
Fe2+	3.116	2.842	2.131	1.631	1.689	1.686	1.553	1.841
Mn	0.081	0.074	0.055	0.053	0.049	0.039	0.035	0.024
Mg	0.542	0.571	1.390	1.565	2.102	2.203	2.572	2.385
Ca	1.933	1.848	1.942	1.766	1.911	1.934	1.880	1.933
Na	0.362	0.332	0.421	0.354	0.323	0.320	0.199	0.209
K	0.419	0.431	0.083	0.120	0.055	0.043	0.065	0.075
Ba	0.000	0.000	0.003	0.000	0.000	0.004	0.000	0.001
OH*	2	2	2	2	2	2	2	2
Total	17.714	17.611	17.449	17.241	17.289	17.301	17.144	17.219
(Ca+Na) (B)	2.000	2.000	2.000	2.000	2.000	2.000	2.000	2.000
Na (B)	0.067	0.152	0.058	0.234	0.089	0.066	0.120	0.067
(Na+K) (A)	0.714	0.611	0.446	0.241	0.289	0.297	0.144	0.218
Mg/(Mg+Fe2)	0.148	0.167	0.395	0.490	0.555	0.567	0.624	0.564
Fe3/(Fe3+Alvi)	0.676	0.737	0.437	0.764	0.564	0.465	0.499	0.218
Amphibole names*	potassian-hastingsite	potassian-hastingsite	ferro-tschermakite	ferri-ferro-tschermakite	magnesio-hornblende	magnesio-hornblende	magnesio-hornblende	magnesio-hornblende
T (C) **	822.41	861.66	683.71	573.43	509.43	493.17	470.14	501.32
P (Kb) **	4.81	3.65	9.87	8.87	6.90	6.85	2.90	4.48

* Leake (1978); Leake, (1984); Mogessie et al. (1990)

**Anderson and Smith (1995); Holland and Blundy, 1994

ME: Microgranular enclave, MMF: Mesoproterozic mafic dyke, NME: Neoproterozoic mafic dyke, PMF: Palaeozoic mafic dyke.

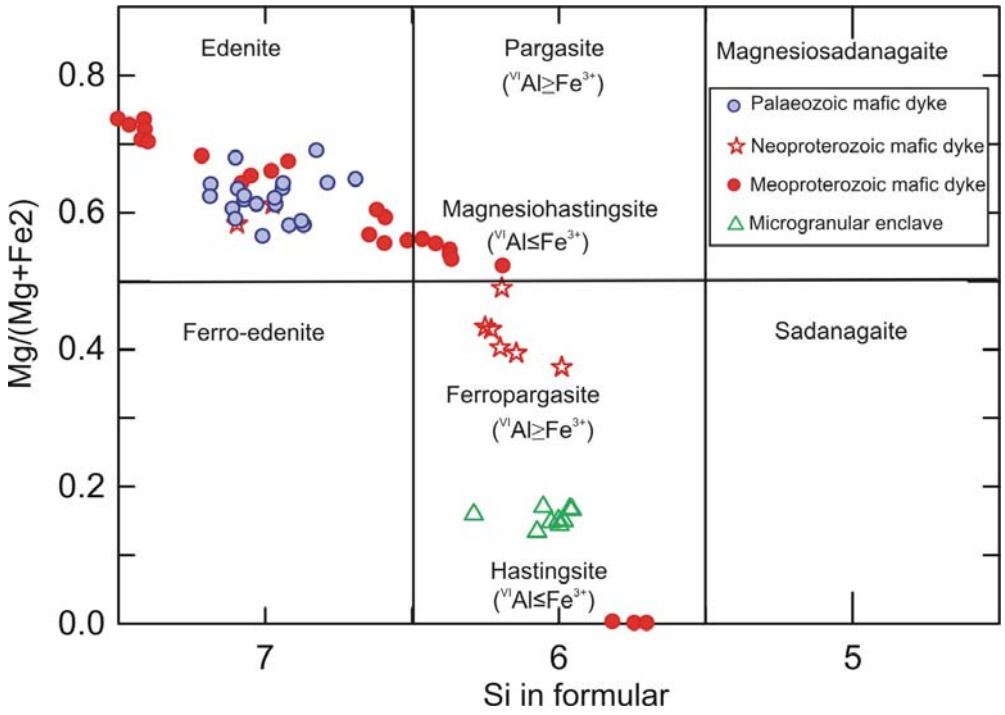

Figure 3.8 Amphibole classifications of Si versus Mg/(Mg+Fe^{2+}) after Leake et al. (2003) of mafic dykes and microgranular enclaves for amphibole which are $Ca_B \geq 1.5$; $(Na+K)_A \geq 0.5$; $Ti < 0.5$.

The composition of magmatic amphibole of microgranular enclaves from the Mt Painter Province is used to estimate pressure following the methods of Anderson and Smith (1995). This analysis shows that the amphiboles formed at pressures ranging from 3.60 to 5.87 kbar and at temperatures ranging from 794 to 944 ºC. The Al_{vi} versus Al_{iv} diagram after Fleet and Barnett (1978; Figure 3.9) shows that most microgranular enclave amphiboles are low pressure Ca-amphibole. Pressures calculated for amphiboles from the Mesoproterozic mafic dyke vary from 0.71 to 10.49 kbar and temperatures from 355 to 606 ºC (Appendix 3). The Al_{vi} versus Al_{iv} diagram (Figure 3.9) suggests that most amphibole plot along low pressure trends with three analyses indicating high pressures interpreted to be due to metamorphism. Amphiboles from the Neoproterozoic mafic dyke show widely varying pressures, from 2.67 to 16.31 kbar and at temperatures ranging from 520 to 772 ºC (Appendix 3). They are typically low pressure Ca-amphibole. Calculations of pressures for amphiboles from the Palaeozoic mafic dykes are between 0.75 to 5.15 kbar and at temperatures ranging from 312 to 546 ºC (Appendix 3). They plot in the low pressure Ca-amphibole area (Figure 3.9). Amphiboles from the Neoproterozoic and Palaeozoic mafic dykes typically having low Nb/La ratios suggest that they are not magmatic

amphiboles. Therefore, the pressures and temperatures that are calculated from compositions of these amphiboles are not realistic.

In the Na+K versus A_{iv} plot (Figure 3.10) after Searle and Malpas (1982), amphiboles from Mount Painter rocks plot along the high temperature trend. Temperature, total pressure and pH_2O are parameters controlling biotite and amphibole Fe/(Fe+Mg) ratios (Wones, 1981). Along with these factors, fO_2 is the most important factor controlling amphibole compositions (Anderson and Smith, 1995). The Fe/(Fe+Mg) in biotite and amphibole has a negative relationship to fO_2. Amphibole Fe/(Fe+Mg) ratios of low fO_2 granite typically exceed 0.40-0.65. Therefore the magmatic amphiboles from microgranular enclaves, which contain Fe/(Fe+Mg) ratios about 0.87, may indicate low fO_2 conditions. The primary hornblendes (magnesiohastingsite) in microgranular enclaves suggest alkali-basalt and calc-alkali series and low f_{H_2O}.

In the sequence of Bowen's discontinuous series, hornblende should crystallize before biotite. However hornblendes from the mafic enclaves formed both before and after biotite which could suggest they were crystallized from K-rich magma with low f_{H_2O} environment.

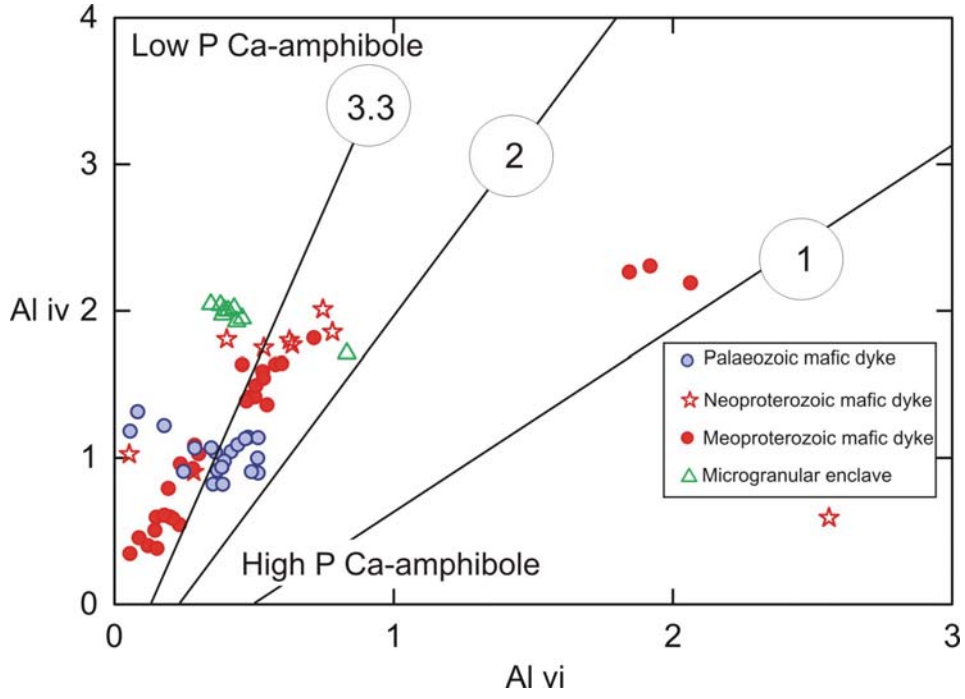

Figure 3.9 A_vi versus A_{iv} diagram after Fleet and Barnett (1978) showing most amphiboles plot within the low pressure Ca-amphibole field.

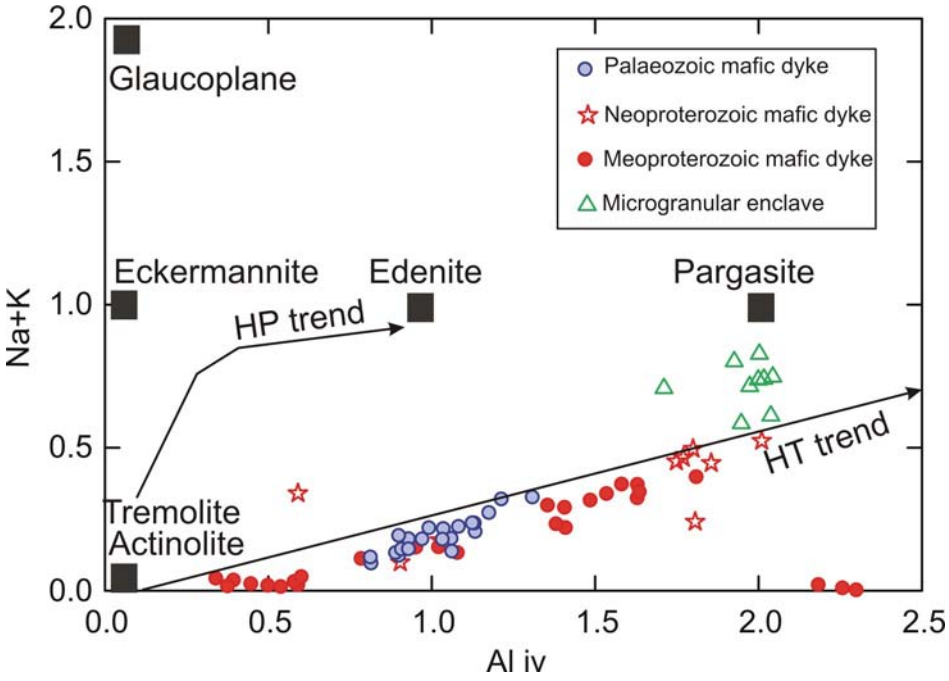

Figure 3.10 Na+K versus A_{iv} diagram after Searle and Malpas (1982) showing amphiboles from the Mount Painter rocks plot along high temperature trend.

Amphiboles from microgranular enclaves and Mesoproterozic mafic dykes contain different levels of trace element contents. The magnesiohastingsite from microgranular enclaves have relatively high trace element concentrations including REE, Y, U and Th compared to Mesoproterozic mafic dykes. REE patterns of the magnesiohastingsite show positive trends with depleted LREE, slightly enriched HREE and strongly negative Eu anomalies (Figure 3.11a). Depleted LREE in the microgranular enclave amphiboles could suggests more extensive equilibration with other phases and strongly negative Eu anomalies could indicate highly fractionatal crystallization involving feldspar. On the other hand, REE patterns of Mesoproterozic mafic dyke amphibole show depleted LREE, flatter HREE and enriched MREE patterns, and negative Eu anomalies suggesting feldspar fractionation crystallization (Figure 3.11b).

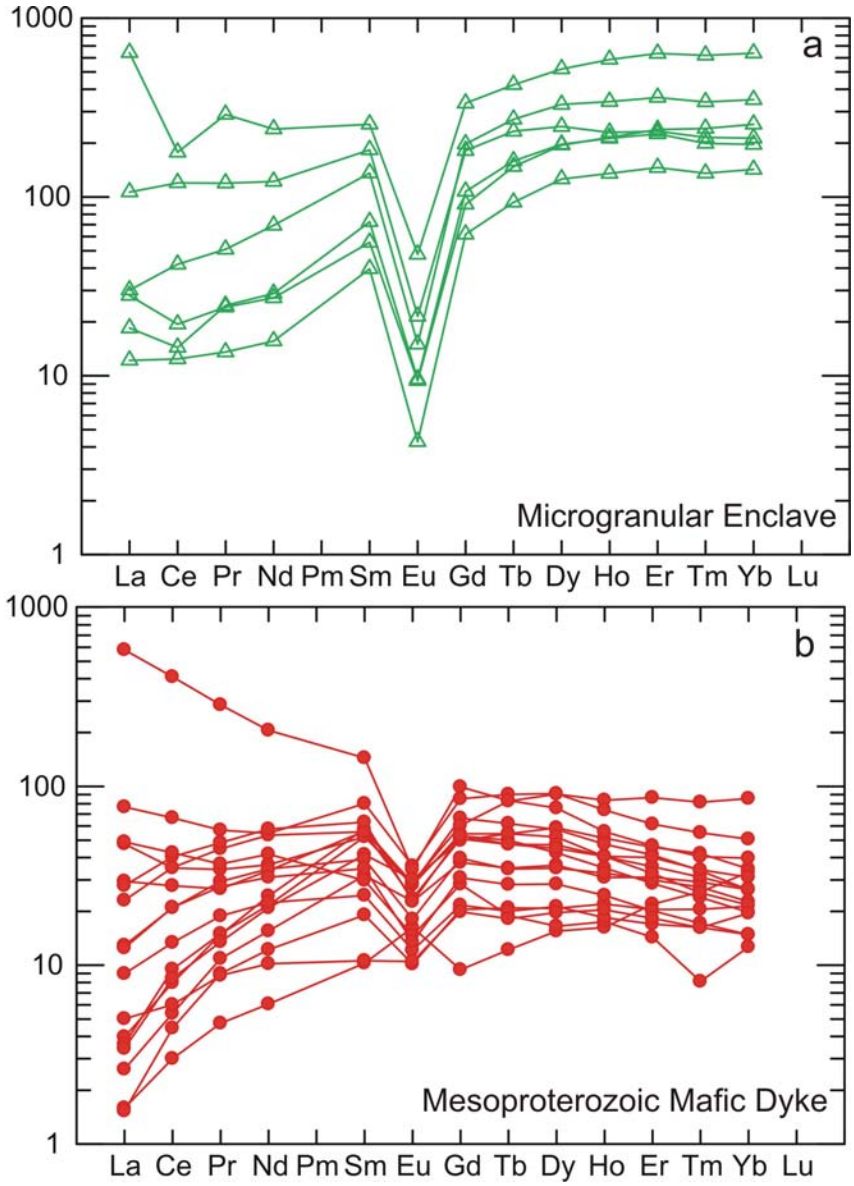

Figure 3.11 Rare earth element concentrations normalised to chondrite values (Sun and McDonald, 1989); a) amphibole REE patterns of microgranular enclave, b) amphibole REE patterns of Mesoproterozoic mafic dyke.

3.1.3 Biotite

Biotite in this study is typically pleochroic pale brown to dark brown, has a strongly to slightly preferred orientation due to deformation. The biotite sometimes shows chloritic alteration. Muscovite may be found in more metamorphosed granites. Zircon, apatite, allanite, U-Th minerals and sphene occur as inclusions in biotite. Dark brown halo damaging by radioactive elements on biotite crystals, which mainly reside in zircon and U-Th minerals,

are common. Biotite in mafic dykes and enclaves is typically subordinate to amphibole.

Biotites from the Pepegoona Volcanics, the Mt Neill, Box Bore, and Yerila granites, microgranular enclaves, and Neoproterzoic and Mesoproterozic mafic dykes were analysed for their major and trace element concentrations. The Fe/(Fe+Mg) ratios of biotite vary among different suites (Table 3.3; Appendix 3). Biotites from felsic rocks including Pepegoona Volcanics, Box Bore and Yerila granites are typically iron-rich; Fe/(Fe+Mg) range from 0.74 to 0.91 with two analyses displaying Fe/(Fe+Mg) ratios of 0.55, so biotites are mainly classified as siderophyllite (Figure 3.12). Mt Neill biotites have the lowest Fe/(Fe+Mg) ratios among felsic rocks, ranging between 0.39 and 0.41. The Fe/(Fe+Mg) ratios of mafic microgranular enclave biotites mainly vary between 0.74 and 0.86 with one analysis of 0.55. Biotite from Mesoproterozic and Neoproterozoic mafic dykes contain relatively lower Fe/(Fe+Mg) ratios than the felsic rocks. The Fe/(Fe+Mg) ratios of Neoproterozoic mafic dyke biotite vary from 0.33 to 0.45 and for Mesoproterozic mafic dykes they are mainly between 0.49 to 0.52, with one analysis having a ratio of 0.87.

Figure 3.13 suggests that most biotites are re-equilibrated primary biotite with some secondary biotites and primary biotites, in particular from the Yerila Granite. These indicate that hydrothermal and/or metamorphic processes affect the chemistry of biotite. Biotite from mafic enclaves and mafic dykes coexist with amphibole (Figure 3.14). The geochemistry of biotites from the Pepegoona Volcanics, Box Bore and Yerila Granite and the mafic enclaves is typical of biotite from peraluminous magma. However, some biotite analyses of the Yerila Granite and mafic enclaves plot in the alkaline field. Biotite compositions in this study do not vary in a sysmatic manner which could suggest they are no longer directly reflecting magmatic compositions.

Table 3.3 Selected biotite analyses to represent the different unit of granitic and volcanic rock from the Mt Painter Province.

Sample	BB25	BB21	SD010	MN092	SD047	MN096	SD004	MN099
Spot	BB2_01	BB21_02	SD10_01	MN92_02	SD47_01	MN97_07	SD04_01	MN99_02
Unit	PV	MN	BB	YG	ME	ME	MMF	PMF
SiO2	32.156	33.625	31.353	34.741	35.209	30.380	36.128	36.013
TiO2	2.790	1.328	2.788	3.048	2.200	1.550	2.447	2.454
Al2O3	17.443	18.511	15.239	15.592	15.535	12.896	14.952	15.472
FeO	28.883	16.867	27.912	27.230	30.040	21.480	18.410	20.136
MnO	0.443	0.223	0.548	0.265	0.444	0.214	0.156	0.121
MgO	3.213	13.852	6.057	4.317	3.505	4.198	12.450	10.606
CaO	0.103	0.000	1.274	0.022	0.062	0.007	0.000	0.047
Na2O	0.038	0.119	0.058	0.048	0.047	0.053	0.037	0.037
K2O	6.870	7.933	4.662	9.573	9.075	7.614	10.125	8.985
BaO	0.059	0.112	0.000	0.039	0.118	0.059	0.421	0.204
H2O*	3.631	3.874	3.573	3.741	3.758	3.141	3.901	3.863
Subtotal	95.628	96.444	93.463	98.617	99.993	81.591	99.029	97.937
Total	95.628	96.444	93.463	98.617	99.993	81.591	99.029	97.937
Si	5.310	5.204	5.262	5.568	5.619	5.800	5.553	5.590
Al iv	2.690	2.796	2.738	2.432	2.381	2.200	2.447	2.410
Al vi	0.706	0.582	0.277	0.514	0.541	0.702	0.263	0.421
Ti	0.347	0.155	0.352	0.367	0.264	0.222	0.283	0.287
Fe	3.989	2.183	3.918	3.650	4.009	3.430	2.367	2.614
Mn	0.062	0.029	0.078	0.036	0.060	0.035	0.020	0.016
Mg	0.791	3.196	1.516	1.031	0.834	1.195	2.853	2.454
Ca	0.018	0.000	0.229	0.004	0.011	0.001	0.000	0.008
Na	0.012	0.036	0.019	0.015	0.014	0.020	0.011	0.011
K	1.447	1.566	0.998	1.957	1.847	1.854	1.985	1.779
Ba	0.004	0.007	0.000	0.002	0.007	0.004	0.025	0.012
OH*	4	4	4	4	4	4	4	4
TOTAL	19.375	19.753	19.387	19.577	19.587	19.463	19.807	19.603
Y total	5.894	6.145	6.141	5.599	5.707	5.584	5.786	5.792
X total	1.481	1.609	1.246	1.978	1.880	1.880	2.022	1.810
Al total	3.395	3.377	3.015	2.946	2.922	2.902	2.709	2.831
Fe/Fe+Mg	0.83	0.41	0.72	0.78	0.83	0.74	0.45	0.52
T(C)*	885.06	870.27	887.83	898.13	865.85	864.96	916.69	906.82

*Luhr et al. (1984); YG: Yerila Granite, ME: Microgranular enclave, MN: Mount Neill Granite, PV: Pepegoona Volcanic, BB: Box Bore Granite, MMF: Mesoproterozic mafic dyke, PMF: Palaeozoic mafic dyke.

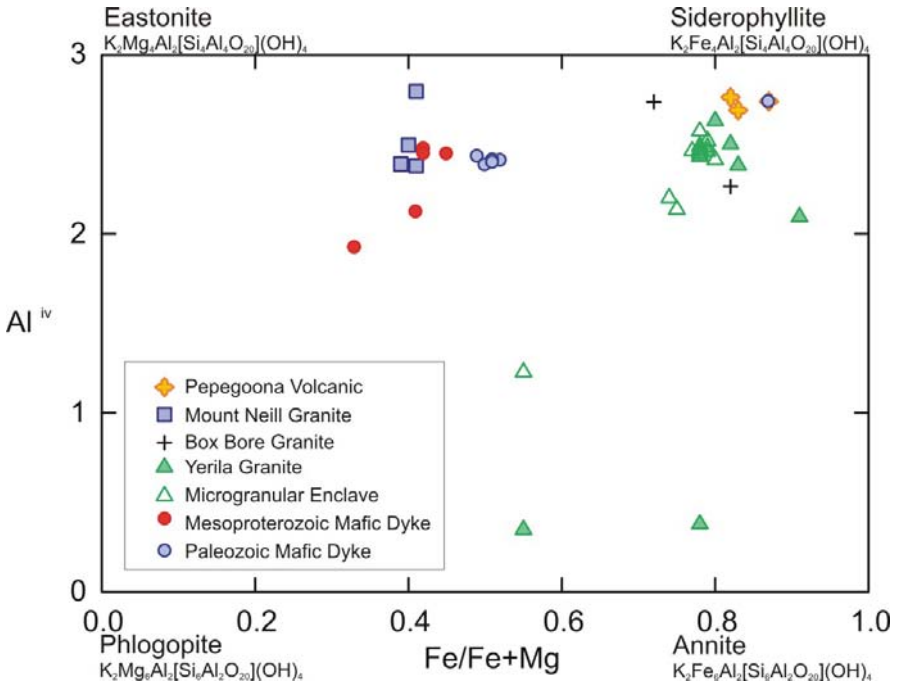

Figure 3.12 Diagram of Fe/Fe+Mg ratio versus Al^{iv} for biotite from mafic and felsic rocks of Mount Painter Province showing various compositions. Felsic rocks are mainly classified as Siderophyllite and mafic rock have composition in between Siderophyllite and Eastonite.

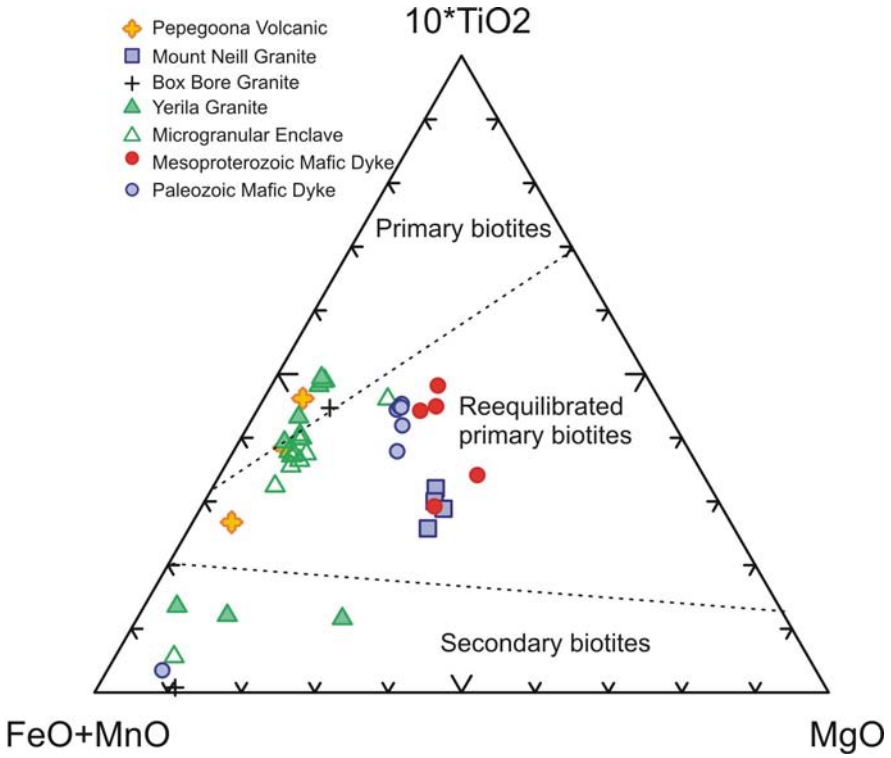

Figure 3.13 Ternary diagram of $10\times TiO_2$-(FeO+MnO)-MgO after (Nachit et al., 1985) for biotites.

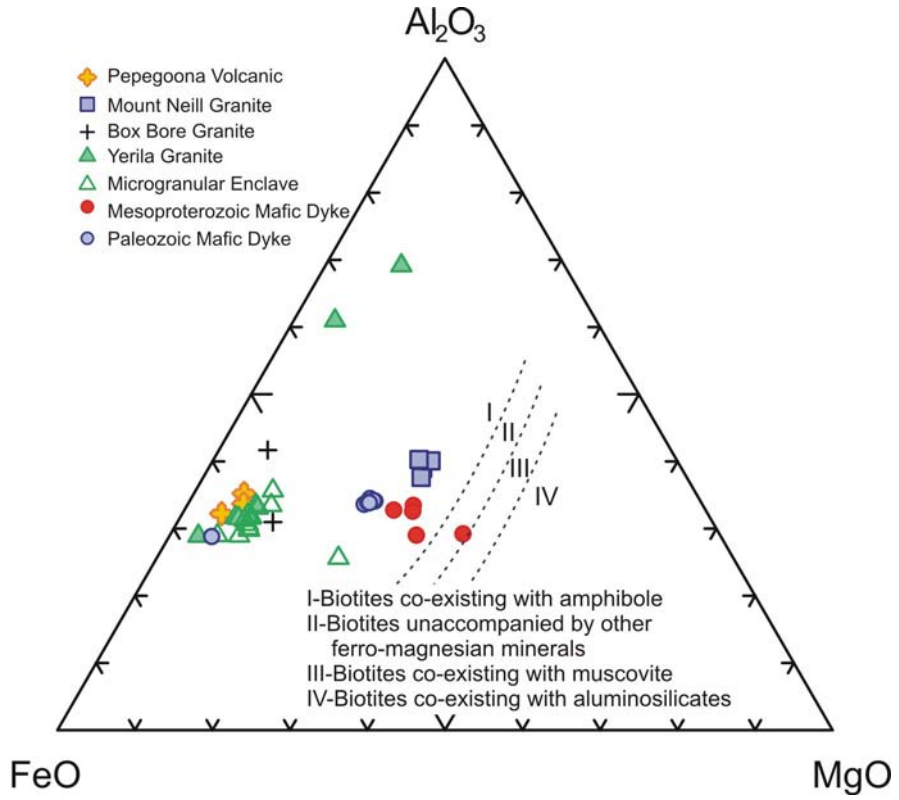

Figure 3.14 Ternary diagram of FeO-MgO-Al_2O_3 after de Albuquerque (1973) for biotite of mafic-felsic igneous rocks from Mount Painter Province, most biotites co-exist with amphibole.

Biotites from the Yerila Granite, microgranular enclaves, Neoproterozic and Mesoproterozic mafic dykes were analysed for trace elements. Their REE patterns are shown in Figure 3.15. REE concentrations in the biotites are commonly low (<1 ppm). However, a few analyses from the Yerila Granite and microgranular enclave biotites contain more than 1 ppm (Appendix 3) which may be found in U-rich granites (Bea, 1996). The REE patterns of the Yerila Granite and microgranular enclave biotites show negative trends with negative Eu anomalies. The microgranular enclave biotites display relatively high fractionation compared to the Yerila Granite biotites, whereas biotites from mafic dykes show very low REEs with flattened flatter REE patterns.

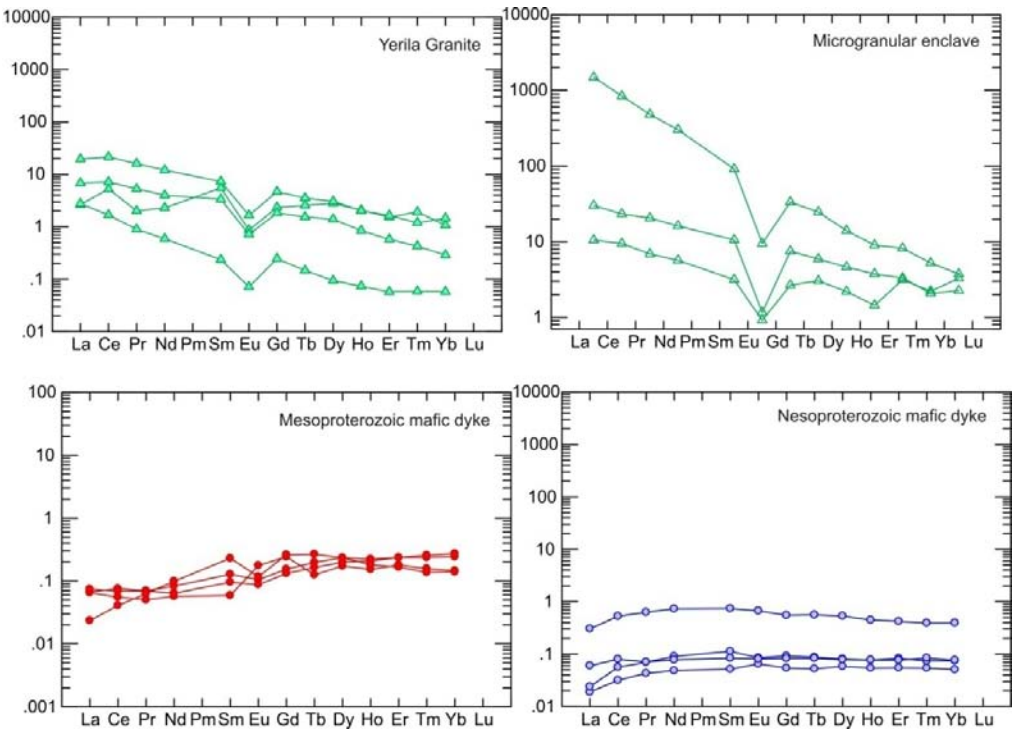

Figure 3.15 Rare earth element concentrations normalised to chondrite values (Sun and McDonald, 1989); a: biotite REE patterns from the Yerila Granite b: biotite REE patterns from Microgranular enclave, c: biotite REE patterns from Mesoproterozoic mafic dyke, d: biotite REE patterns from Nesoproterozoic mafic dyke.

3.2 Accessory minerals

3.2.1 Zircon

Zircons are found in most granitic and mafic rocks as euhedral to subhedral crystals enclosed in biotite, amphibole and feldspar and rarely in quartz. Radioactive damage haloes are frequently found around zircon grain boundaries. However, zircon is absent from the Palaeozoic mafic dykes. Magmatic zircons from different suites of rocks in this study typically have different morphologies and abundance. Detailed zircon morphology is discussed in Chapter 4 Geochronology. Trace-element chemical compositions of the zircons in this study were studied by using LA-ICMPS at the Adelaide microscopy (detailed methodology in Appendix 1 and result in Appendix 3).

Major-element compositions of the Yerila Granite zircons show a narrow range (ZrO_2 ranging from 60.22 to 68.45 wt%; SiO_2 ranging from 30.23 to 33.84 wt%; and HfO_2 ranging from 1.35 to 2.23 wt%; Wülser, 2009).

Trace element concentrations of zircons from different suites show variable abundances (Table 3.4). Zircons from microgranular enclaves, the Yerila Granite and mafic dykes are extremely enriched in U and Th. Zircons from other felsic and mafic rocks have lower U and Th contents than the Yerila Granite and microgranular enclave zircons, however they are higher than zircon from normal granitic rocks which average 764 ppm U and 368 ppm Th (Belousova et al., 2002).

Generally, igneous zircons have Th/U ratio's within the range 0.4-1.0 (Hoskin and Ireland, 2000) and metamorphic zircon has low Th/U ratio (less than 0.1; e.g. Hoskin and Ireland, 2000; Rubatto, 2002; Hartmann and Santos, 2004). Based on values of Th/U ratios, zircons in most samples are magmatic zircons having Th/U ratios greater than 0.4; except for a few analyses from mafic dykes showing low values that may be indicated metamorphism (see all data in Appendix 3). Some analyses showing high Th/U ratios (e.g. from sample SD057 and SD060) could indicate that the zircons formed by late stage crystallization of zircons from mafic magma (Heaman et al. 1990).

REE concentrations and patterns of zircons are governed by magma compositions, coexisting phases and oxygen fugacity (Koreshkova et al., 2009). Zircons from different suites exhibit various REE contents and patterns. Thus, the different REE patterns of the zircons are interpreted to be the result of different magma compositions. The REE patterns of these zircons have slightly depleted LREE patterns (Figure 3.16a, c, e, g and i) similar to the average granitoid (Figure 3.16b, d, f, h and j). Moderately enriched HREE patterns, positive Ce anomalies and negative Eu anomalies are found in all analyses. Zircons from the Yerila Granite and microgranular enclaves show relatively flat HREE patterns compared to other rock groups.

Table 3.3 Selected zircon analyses obtained by LA-ICPMS to represent the different unit of granitic and volcanic rock from the Mt Painter Province.

Sample	SD049	SD060	MN003	MN029	SD015	MN101	SD028	MN084	SD051
Spot	S49MYZ2	SD60YZ3	MN03VLZ2	MN29MNZ2	SD15BBZ5	MN10TPZ5	SD028MZ4	MN84MNZ2	SD051MDZ3
Unit	ME	YG	PV	MN	BB	TP	WG	MMF	NMF
Ba	1156	65	9	2	110	58	475	1	724
Ce	46151	5805	51	13	258	507	501	27	3358
Dy	220742	2143	465	107	2107	3200	37867	139	20387
Er	306184	2630	610	175	2363	2649	72204	210	27375
Eu	1768	178	2	1	15	79	28	0	428
Gd	68971	994	134	31	488	984	6727	32	6429
Ho	73586	641	150	39	573	740	14846	47	6895
La	9011	2033	7	2	44	43	99	2	564
Lu	88395	807	161	61	569	665	27107	68	5155
Nb	70449	241	12	5	643	568	473	11	169
Nd	33475	2637	30	6	298	493	456	7	3441
Pb	25756	2052	75	18	101	260	3713	20	1963
Pr	5426	617	4	1	50	87	51	1	528
Sc	199570	2309	344	258	561	763	87871	348	5161
Sm	26430	668	34	7	239	452	964	8	2466
Sr	820	254	2	1	73	100	227	1	112
Ta	1708	76	3	1	53	20	284	4	77
Tb	19403	223	41	9	190	333	2636	11	1712
Th	225845	12581	679	69	1375	633	29443	160	26146
Tm	63916	572	126	36	525	527	16947	45	5165
U	442942	23290	1077	178	3482	2048	97359	603	33238
Y	1981487	19135	4356	1167	13370	20582	438922	1441	201808
Yb	577575	5024	1094	321	4465	4526	168759	408	40252
Th/U	0.51	0.54	0.63	0.39	0.39	0.31	0.30	0.26	0.79

YG: Yerila Granite, ME: Microgranular enclave, MN: Mount Neill Granite, PV: Pepegoona Volcanic, WT: Wattleowie Granite, TP: Terrapinna Granite, BB: Box Bore Granite, MMF: Mesoproterozic mafic dyke, NME: Neoproterozoic mafic dyke.

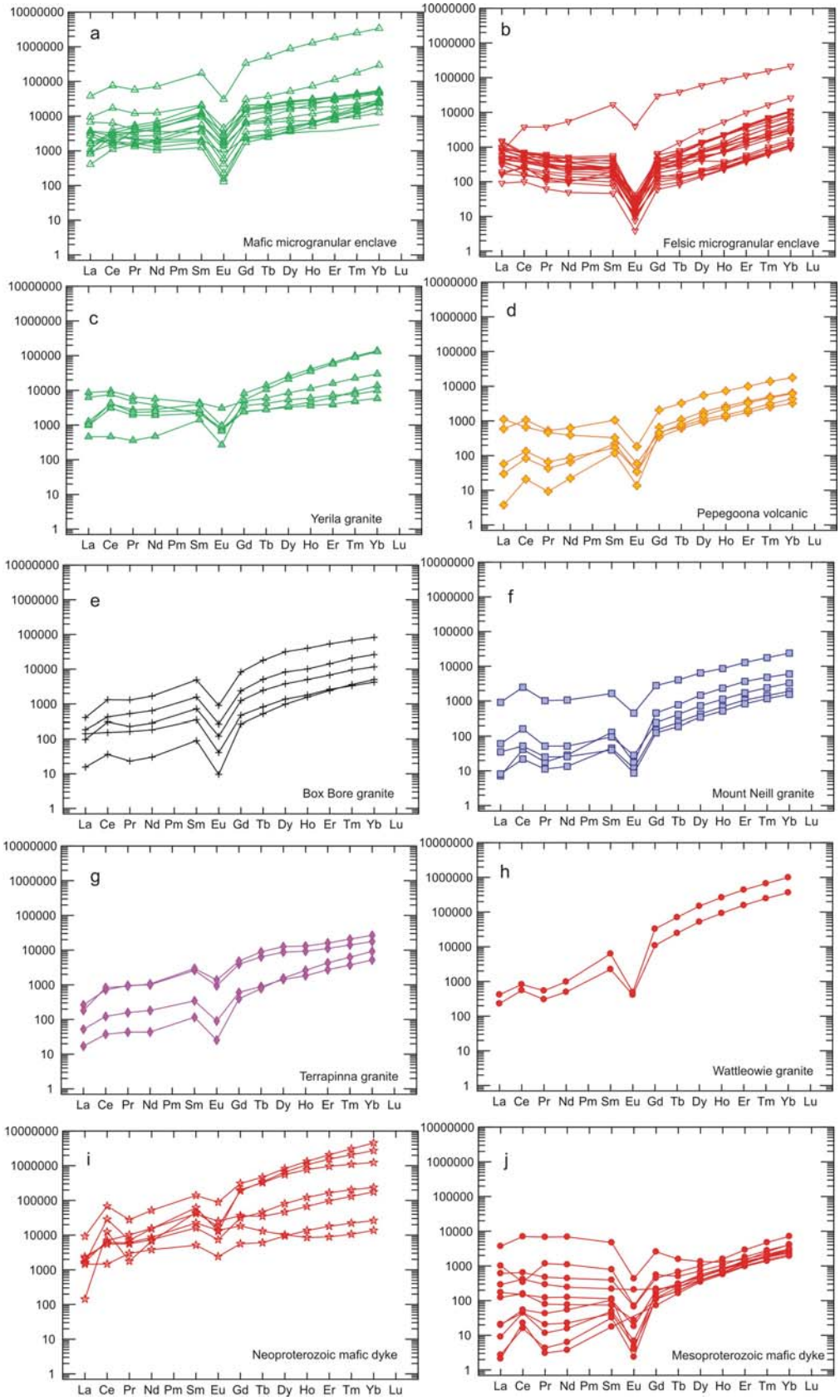

Figure 3.16 Rare earth element concentrations of zircons from MP mafic and felsic igneous rocks normalised to chondrite values (Sun and McDonald, 1989).

The abundance of REEs in microgranular enclave and Yerila Granite zircons might increase during crystallization. A negative Eu anomaly, which is a common characteristic of granitic zircons (e.g. Murali et al, 1983; Hoskin and Ireland, 2000), could reflect coexistence of zircon and K-feldspar (Murali et al, 1983; Hinton and Upton, 1991) or to Eu depletion of the rock as a whole (Schaltegger et al., 1999), moreover it also reflects the presence of Eu^{2+} in the melt related to reducing conditions (Hoskin and Schaltegger, 2003). Generally, a positive Ce anomaly in igneous zircons has been suggested to indicate an abundance of Ce^{4+}, or oxidising conditions, which allows Ce^{4+} to readily substitute for Zr^{4+} (Hoskin and Schaltegger, 2003). However, a small positive Ce anomaly in meteorites, lunar and mantle-affinity zircons is consistent with reducing conditions during zircon formation. Based on the negative Eu and small positive Ce anomalies the zircons from the Mt Painter Province are interpreted to have formed under reducing conditions. Lower HREE enrichment in the Yerila Granite and microgranular enclave zircons compared to other groups could be caused by sub-solidus recrystallization (Hoskin and Black, 2000; Rubatto, 2002). Normally, melts enriched in incompatible elements such as the LREE, U and Th are related to fractional crystallization (Hoskin, 2005) which results in enrichment in incompatible elements at the outer part of the crystal relative to the inner part. The analyses of large zircon grains from microgranular enclaves (Sample SD047; Table 3.4) do not show consistent patterns, with increasing U and Th concentrations found both toward the cores and toward the rims of different grains. The zircons from the Mt Painter Province are enriched in REE, U and Th, in particular zircons from the Yerila Granite and microgranular enclaves have similar patterns to hydrothermal zircon from the Boggy Plain zoned pluton aplite, eastern Australia (Figure 3.17; Hoskin, 2005). This suggests that zircon from the Mt Painter Province granites could have precipitated from melts evolved from magma during the final stages of crystallization.

Table 3.4 U and Th contents anf Th/U ratio of core and rim zircons from sample SD047 (microgranular enclaves).

Spot	Core/Rim	Th (ppm)	U (ppm)	Th/U
1	Core	3495	4392	0.8
	Rim	406	1581	0.3
2	Core	2412	8430	0.3
	Rim	155	1034	0.1
3	Core	1107	1961	0.6
	Rim	1990	9989	0.2
4	Core	6858	4533	1.5
	Rim1	3840	5772	0.7
	Rim2	1530	12466	0.1
5	Core	1593	4493	0.4
	Rim	1083	6033	0.2
6	Core	8693	7336	1.2
	Rim1	4811	12376	0.4
	Rim2	3594	27522	0.1
7	Core	4448	10487	0.4
	Rim	714	5556	0.1
8	Core	1779	1408	1.3
	Rim	1905	12468	0.2
9	Core	3382	3366	1.0
	Rim1	358	1916	0.2
	Rim2	817	3437	0.2

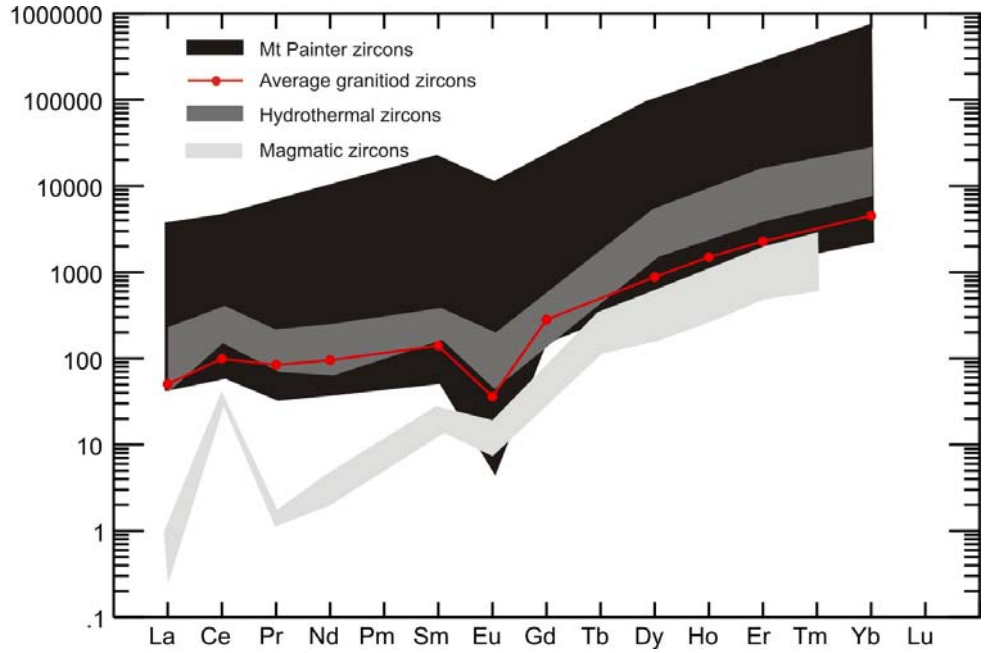

Figure 3.17 REE patterns of zircons from mafic and felsic magmatic rocks of the Mt Painter Province compare to magmatic and hydrothermal zircons from (data from Hoskin, 2005) and average granitiod zircon (from Belousova et al, 2002).

3.2.2 Allanite

Allanite is typically an important host for U and Th and is the main repository for LREE in the continental crust (Gromet and Silver, 1983; Bea 1996). Studying the geochemistry of allanites could assist in determining the genesis of the enriched U-Th grainitic rocks of the Mt Painter Province.

In this study, allanites are found in both felsic and mafic rocks; however they are more abundant in the Yerila Granite and its enclaves. The allanites are typically large euhedral to subeuhedral and yellow to yellowish brown crystals (average of 3 mm and up to 5 mm). The allanite crystals contain fissures and tracks of alpha-particles, a texture like that of primary allanite in A-type granites from Graciosa Province, Brazil (Vlach and Gualda, 2007), and may indicate replacement of metamict allanite. Darker zones generally appear along fractures and boundaries between allanite and other minerals. These suggest that the allanites were affected by hydrothermal alteration, which was later increased by radioactive damage and related chemical transformations (Poitrasson, 2002). However, some allanite grains preserve patchy zoning indicating a primary magmatic origin. Allanite in the mafic dykes is smaller (<100 μm) and more affected by hydrothermal alteration than the Yerila Granite allanites. Apatite, zircon, ilmenite and magnetite inclusions and rims of epidote are observed in these allanites. The allanite is found as inclusions in biotite and may itseft contain biotite inclusions. This evidence is interpreted to suggest that the allanites began to crystallize at about the same time as biotite but after feldspar, amphibole, and apatite. Fluorite is found surrounding allanite grains, having formed from late F-rich fluids.

Allanites from Yerila Granite and micrograular enclaves were analysed for their chemical compositions in this study. They are much enriched in Ce compare to other REE (Table 3.5). Based on the classification of Ercit (2002) using major REE contents of allanite-(Ce), allanite-(La) and allanite-(Y), the allanite grains are identified as allanite-(Ce). These allanites can be further classified further more as Mn-poor allanite-(Ce) showing Mn<0.14 apfu (atoms per formula unit; Table 3.5 and Appendix 3) which is linked to the magmatic series granitic rocks (Hoshino et al., 2006). Wülser

(2009) analysed the Yerila Granite allanites and suggested that the allanite compositions are between allanite-Ce and ferriallanite-(Ce). The ThO_2 content in the Yerila Granite and microgranular enclave allanites widely ranges from 0.90 to 2.91 wt% and from 0.96 to 2.64 wt%, respectively. The U_2O content ranges from 0.04 to 0.26 wt% for enclave allanites and 0.04 to 0.29 wt% for Yerila granite allanites.

The allanite from the Yerila granite and its enclaves contain high concentrations of trace elements. The total of REE, Th and U of these allanite are generally high (up to 168494 ppm; Table 3.5).

Table 3.5 Selected allanite analyses obtained by LA-ICPMS from the Yerila Granite and micrgranular enclave from the Mt Painter Province.

Sample	MN096	MN096	MN096	MN096	MN092	MN092	MN092	MN092
Spot	MN96ALN1	MN96ALN2	MN96ALN5	MN96ALN6	MN92ALN3	MN92ALN4	MN92ALN5	92ALC0S1
Unit	ME	ME	ME	ME	YG	YG	YG	YG
Ba	390	150	78	55	93	112	91	230
Ce	48386	122578	85038	86664	54644	110231	67560	79755
Cr	46	48	45	26	15	26	26	37
Dy	2975	1581	1314	681	451	1564	1297	1471
Er	1232	486	421	218	152	575	435	540
Eu	48	63	43	27	32	72	71	83
Ga	87	237	177	179	141	144	145	180
Gd	2115	3250	2316	1345	823	2288	2091	2360
Ho	499	225	192	99	67	253	195	238
La	1780	67703	46228	54931	41832	27789	30904	41305
Lu	141	42	37	20	16	52	38	50
Mn	2468	2332	1969	2385	854	2278	2204	2078
Nb	14	28	42	26	156	449	111	333
Nd	3846	39714	27546	22020	14080	19121	21070	23074
Pb	1951	2667	2233	1019	824	1717	1310	1793
Pr	887	12264	8552	7690	4734	5800	6449	7104
Rb	457	9	18	5	8	11	8	15
Sc	69	54	54	25	49	206	129	149
Sm	1381	5395	3708	2337	1464	3200	3168	3478
Sr	110	1431	1354	892	2363	981	1117	1144
Tb	435	350	270	145	94	294	252	289
Th	64089	16854	15014	9820	10056	15234	11014	20383
Ti	2045	11242	10698	13474	6319	9123	6438	9100
Tm	151	55	47	26	20	67	49	63
U	7845	2170	568	347	648	2049	2272	2441
V	193	221	196	174	51	208	453	292
Y	9474	6631	4996	2783	2008	6797	6126	5533
Yb	943	329	284	152	108	386	284	368
Zr	191	651	660	84	6936	2310	159	4794
Σ REE	62846	241401	167123	168494	113659	165455	127092	139844

The chondrite-normalised REE patterns of the allanites from the Yerila Granite and microgranular enclaves display a similar pattern with enriched LREE, depleted HREE and negative Eu anormalies (Figure 3.18), which are typical for allanite-(Ce). Decreasing LREE in some allanite analyses may be caused by hydrothermal alteration by oxidizing fluids (Poitrasson, 2002). The allanite in this study is overgrown by epidote, which is REE-poor, but the reverse is not seen. The allanite REE patterns are very similar to the whole-rock Yerila Granite and microgranular enclave, which suggest that the allanites contain the majority of the REE in the rocks. The textural relationships between allanite and epidote could be used for estimate minimum crystallization temperature for allanite. Early allanite crystallized at temperature exceeding the stability field of epidote (above 700 °C; Oberli et al., 2004).

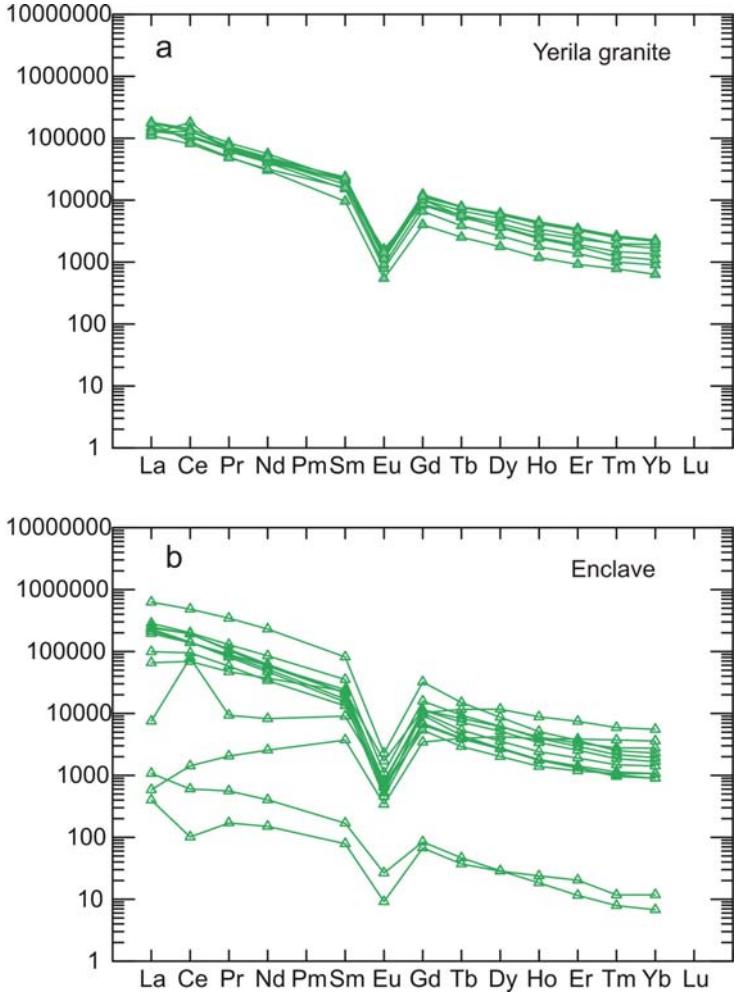

Figure 3.18 Rare earth element concentrations of allanites normalised to chondrite values (Sun and McDonald, 1989) from a) the Yerila granite and b) microgranular enclave.

3.2.3 Apatite

Apatite is one of the major hosts for REE, Sr, Y and Mn in granites and other rock types and typically forms as an early magmatic phase (O'reilly et al., 1991; Casillas et al., 1995). Apatite is present in all rock units in the Mt Painter Province mafic and felsic rocks but is most common in mafic dykes. It appears as euhedral to subhedral needles and grains in various size and is found as inclusion in biotite, quartz, feldspar, allanite and zircon.

Apatites from the Yerila Granites are fluorine-rich (fluroapatite; Wülser, 2009) with Y-enriched compositions (Y_2O_3 content up to 2.5 wt%; Wülser, 2009). Two populations of fluoroapatite including Y-poor and Y-rich and Si-bearing populations are found in the Yerila Granites (Wülser, 2009).

Apatites from the Yerila Granite, microgranular enclave and Mesoproterozoic mafic dyke were analysed for their trace elements and they typically contain low concentrations of REEs (Table 3.4).

REE patterns of the apatites are mainly depleted in LREE, enriched in HREE and have negative Eu anomalies, however, some apatites from the microgranular enclaves and mafic dykes show negative REE trends (Figure 3.19). The behaviour of HREE and LREE in apatites strongly reflects the crystallization environment in host rocks (Belousova et al., 2001). Enriched LREE and steeper LREE patterns may indicate more oxidised granites and high degrees of fractionation (Belousova et al., 2001) and are characteristic of I-type granites (Broska et al., 2004). On the other hand, apatite REE patterns with LREE depletion and HREE enrichment may indicate a more reduced condition, which is found within the Yerila Granite, microgranular enclaves and mafic dykes. Enriched HREE in the REE pattern of the apatites is common in S-type and A-type granites (Broska et al., 2004). Sr contents in apatites, which vary from low to high contents (Appendix 3) could indicate different degrees of fractionation.

Table 3.3 Selected apatite analyses obtained by LA-ICPMS from the Yerila Granite, microgranular enclave and mafic dyke from the Mt Painter Province.

Sample	BB06	BB06	MN092	MN092	MN092	MN092	MN092	MN096	MN096
Spot	BB6AP1	BB6AP2	92pc1s1	92pc3s1	92pc4s1	MN92AP1	MN92AP3	MN96AP4	MN96AP6
Unit	Mafic Dyke	Mafic Dyke	Yerila Granite	Yerila Granite	Yerila Granite	Yerila Granite	Yerila Granite	Enclave	Enclave
Ce	489	744	172	658	497	381	784	119	69
Co	<0.30	<0.240	3	1	1	0	<0.21	<0.16	<0.072
Cu	<0.68	<0.64	59	3	1	<0.62	<0.59	<0.149	<0.084
Dy	227	276	490	2011	1805	2861	2210	612	360
Er	95	120	430	1812	1386	2180	1770	450	264
Eu	32	30	15	39	37	56	63	6	4
Ga	0	1	4	10	18	0	1	0	0
Gd	295	331	206	878	1053	1643	1361	352	207
Ho	40	50	128	528	435	711	561	143	83
La	147	381	49	192	113	111	213	26	15
Lu	7	8	69	292	205	312	312	65	40
Nb	0	0	1	2	1	0	0	0	0
Nd	603	618	173	711	873	898	1166	213	118
Pb	4	4	7	47	19	27	22	1	2
Pr	93	106	31	119	117	100	170	29	16
Rb	<0.35	<0.34	3	7	85	2	2	2	0
Sm	234	237	95	405	550	726	659	149	85
Sr	312	275	31	30	26	21	20	9	6
Tb	39	46	54	218	226	348	271	75	44
Th	2	3	71	540	317	725	567	155	122
Tm	11	13	63	278	204	328	289	65	39
U	28	30	32	171	117	229	184	61	46
Y	1159	1346	4089	17226	13368	22265	20770	4757	2678
Yb	54	65	419	1878	1352	2083	1918	442	266
Zr	0	0	11	58	7	2	4	0	0
Σ REE	3488	4329	6500	27565	22313	35383	32812	7584	4363

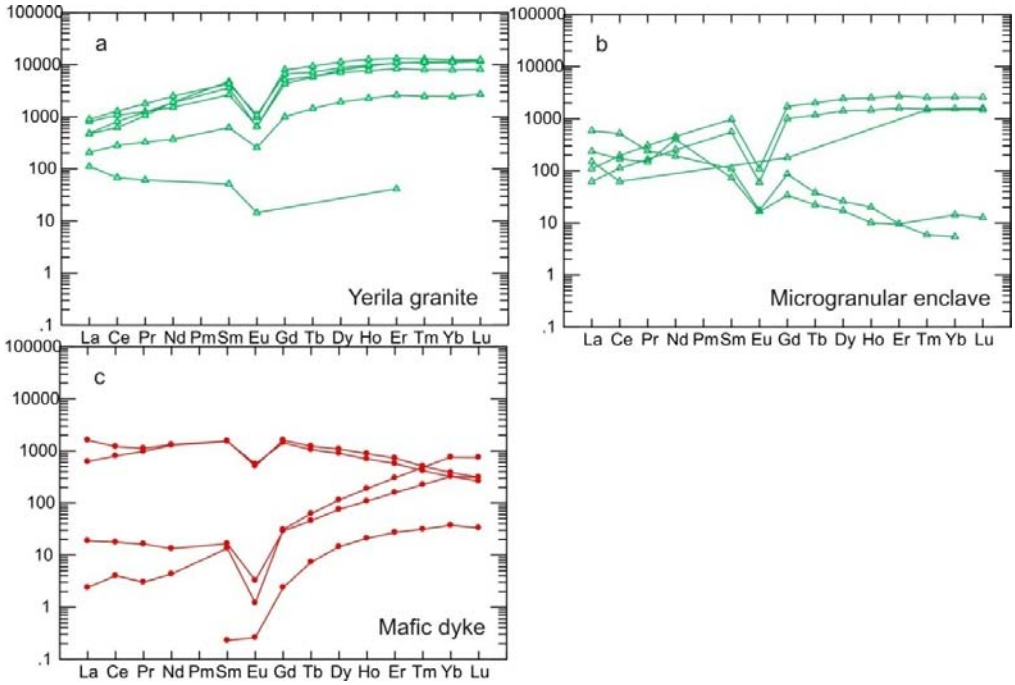

Figure 3.19 Rare earth element concentrations of apatites normalised to chondrite values (Sun and McDonald, 1989) from a) the Yerila Granite; b) microgranular enclaves and c) mafic dyke.

3.2.4 Ti minerals

Ti minerals are found in both mafic and felsic rocks. They are characterised by anhedral to subhedral morphologies. Ti minerals from the Yerila Granite and microgranular enclaces are typically colourless in thin section but are reddish brown to opaque in samples from mafic dykes. The Ti minerals occur within allanite, plagioclase, amphibole, quartz, biotite and K-feldspar.

Chemical compositions of Ti minerals were analysed by EMP and LA-ICPMS (Appendix 1). Ti minerals identified in mafic dykes, including rutile (TiO_2), ilmenite ($FeTiO_3$) and titanite ($CaTiSiO_5$) are typically altered. Colourless Ti minerals including sphene or titanite and altered ilmenite found in the U- and Th-enriched Yerila Granite and microgranular enclaves have unusual compositions, having high Y and REE contents (Y_2O_3 up to 2.5 wt%), moderate Al_2O_3 and Fe_2O_3 concentrations (average of 5.8 and 1.6 wt%, respectively) and high fluorine contents (>2 wt%; Wülser, 2009).

Sphenes from the microgranular enclaves have U and Th contents ranging from 34 to 148 ppm and 53 to 198 ppm, respectively (Appendix 3).

The Yerila Granite sphenes have higher U and Th contents, ranging from 52 to 531 ppm and 4 to 300 ppm, respectively. Yerila Granite ilmenites contain high U and Th concentrations from 3752 to 5421 ppm and 155 to 271 ppm respectively. Ti minerals from mafic dykes have high U (up to 86338 ppm) and Th contents (up to 10386 ppm; Table 3.4).

Table 3.4 Selected Ti minerals analyses obtained by LA-ICPMS from the Yerila Granite, microgranular enclave and mafic dyke from the Mt Painter Province.

Sample	MN096	MN096	MN092	MN092	MN090	SD007	SD007	BB06	BB06
Spot	MN96TIN3	MN96TIN7	MN92TI3	MN92TI4	90ilc1s1	SD07TIN1	SD07TIN4	MN99TI1	MN99TI2
Unit	ME	ME	YG	YG	MF	MF	MF	MF	MF
Ba	1	8	3	3		10068	10068	1	1
Ce	1625	601	710	289	6180	370	13291	7707	2211
Co	0	2	<0.34	0	86728	1109	1439	49523	41167
Cr	14	11	7	8	19987	37626	195398	296750	48782
Cu	2	2	4	6	10070	6951	32344	18035	348
Dy	3510	2523	2458	2014	237	172	1358	1058	901
Er	2086	1591	1519	1751	222	159	786	650	519
Eu	52	31	41	34	77	77	406	244	294
Ga	8	10	8	9	1193	1927	1444	3422	414
Gd	2326	1329	1320	680	630	320	1891	885	808
Hf	25	12	11	9	237	2415	11932	219	6147
Ho	720	534	521	527	69	60	355	227	171
La	272	109	229	92	3891	337	8084	4084	725
Lu	230	181	178	275	62	60	298	93	71
Nb	6253	5762	5646	6839	371219	844036	6341536	59967	12004
Nd	3015	1141	875	385	2320	253	5408	4534	2121
Ni	<0.30	1	<0.69	<0.66	18591	700	3468	28496	2658
Pb	28	63	94	102	41761	237	8855	1729	1182
Pr	427	159	129	61	718	43	1303	1089	392
Rb	2	7	3	4	136	22493	4414	1141	1608
Sc	18	13	36	57	6044	245010	823419	11278	772
Sm	1609	755	784	303	645	269	1428	1133	718
Sr	5	9	7	6	5074	1080	25409	3339	301
Ta	683	624	1732	735	17886	67676	769546	2509	495
Tb	482	322	313	205	55	42	308	174	137
Th	148	48	303	191	155	202	10386	212	600
Tm	314	240	246	310	65	59	277	110	70
U	186	198	532	345	3753	11420	86338	444	373
V	137	122	144	117	1919888	790510	4264862	172745	32255
Y	20869	15326	15583	16236	865	88	5044	5522	4830
Yb	2005	1543	1602	2145	319	170	1401	666	508
Zr	239	135	167	220	5610	82655	419633	7804	283695
ΣREE	42780	31004	31278	31761	385253	846262	6377767	83610	24356

ME:Microgranular Enclave, YG: Yerila Granite, MF: Mafic Dyke

REE patterns of Ti minerals are shown in Figure 3.20. Sphenes from the Yerila Granite and microgranular enclaves show predominately LREE depleted, MREE enriched patterns and negative Eu anomalies (Figure 3.20a and b). Chondrite normalised REE patterns that display relative enrichment of Ce over La are typical for alkaline rocks (Hode and Ulf, 2005). Depleted REEs in some analyses of Ti minerals, which occur as residual or fractionating phases during partial melting or fractional crystallization in the derived magmas, can be found.

The sphene from the Yerila Granite were formed at low to moderate pressures at high temperatures (<6 kbar; >400 C) corresponding to late-to post-magmatic conditions (Wülser, 2009).

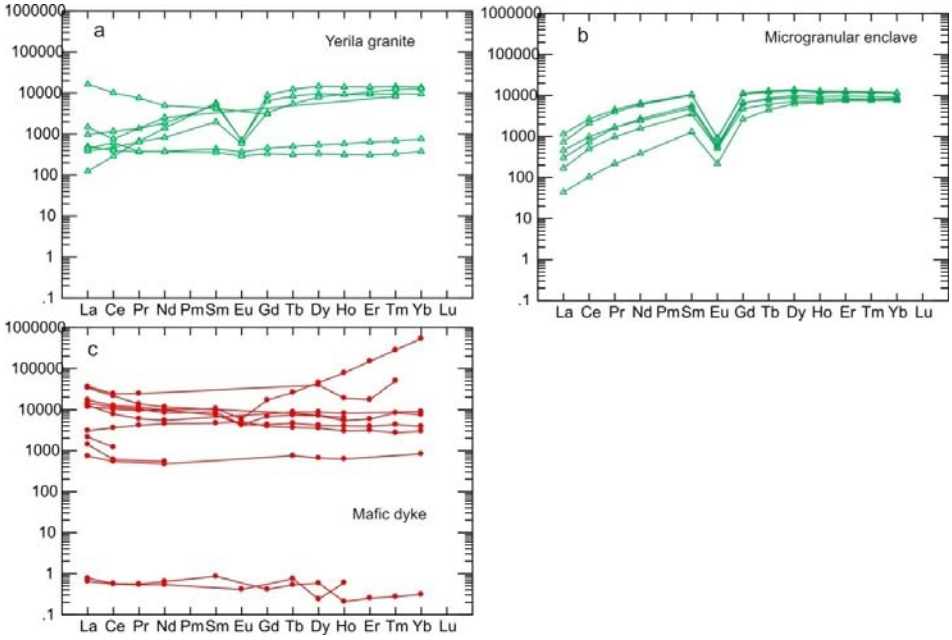

Figure 3.20 Rare earth element concentrations of Ti-minerals normalised to chondrite values (Sun and McDonald, 1989) from a) the Yerila Granite; b) microgranular enclaves and c) mafic dyke.

3.2.5 U-Th minerals

U-Th minerals occurring as primary disseminated phases are found as minor accessory constituents in the HHP mafic and felsic rocks of the Mt Painter Province. They are more abundant in the Yerila Granite and microgranular enclaves and are found at lesser levels in other suites. The U-Th minerals of the Yerila Granite and microgranular enclaves typically occur as euhedral to anhedral, solitary crystals, with grain sizes ranging between 10 to 100 μm. They are hosted by amphibole, biotite, quartz, plagioclase and K-

feldspar and often are adjacent to zircon and apatite. They have generated radioactive damage zones on biotite, feldspar and amphibole at grain boundaries. Wülser et al. (2005) suggested that the original magmatic U-Th minerals include uranothorite, Th-enriched uraninite, uraninite, thorite, coffinite and uraniferous apatite from the HHP granite of Mt Painter Province.

Table 3.5 shows trace element concentrations in the U-Th minerals. REE patterns of U-Th minerals from the Yerila Granite and microgranular enclaves are shown in Figure 3.21. They display negative patterns (enriched LREE and depleted HREE) with negative Eu anomalies (Eu/Eu* = 0.09-0.30). The U-Th minerals of Yerila Granite show positive Ce anomalies. Negative Eu anomaly in the REE patterns indicates reducing conditions at the mineral forming stage. The REE patterns are similar for both the U-Th minerals and the host Yerila Granite.

Wülser (2005) suggested that the original magmatic U-Th minerals were overprinted by a late-magmatic metasomatic event. Flow of F-rich fluids through the rocks during a Late-Ordovician magmatic-thermal event played an important role in the U-Th-rich rocks forming secondary U-Th minerals, which replaced primary U-Th minerals within fracrure in allanite, apatite, titanite/ilmenite, zircon, K-feldspar and amphibole (Elburg et al., 2003).

3.3 Discussion

3.3.1 Relationships between accessory minerals and whole rocks

In the Mesoproterproterozic HHP rocks from the Mt Painter Province, most of the LREEs reside within allanite and U-Th minerals, with the remainder in biotite, feldspar and amphibole. Most of the HREEs reside within zircon, apatite, Ti minerals and amphibole. Most of the Y resides in accessory mineral including apatite, allanite, Ti-minerals, U-Th mineral and zircon with lees amounts in amphibole. Feldspar is the most important Eu reservoir containing most of the Eu. Th is mainly found within accessory minerals such as allanite, U-Th minerals, Ti minerals (sphene) and zircon. U mainly contain within zircon, U-Th minerals, allanite and Ti minerals with minor in apatite.

Table 3.5 U-Th mineral analyses obtained by LA-ICPMS from the Yerila Granite and microgranular enclave from the Mt Painter Province.

Sample	MN092	MN092	MN092	MN096
Spot	MN92U1	MN92U3	MN92UZ3	MN96U
Unit	Yerila Granite	Yerila Granite	Yerila Granite	Enclave
Ba	22	33	3	660
Ca	1	1	1	8
Ce	850	6850	548	40604
Co	4	1	0	56
Cr	2	36	0	44
Cu	9	7	2	133
Dy	39	100	92	477
Er	13	34	57	141
Eu	6	8	5	99
Ga	12	13	1	259
Gd	56	174	83	1358
Hf	35	26	9	843
Ho	6	16	20	72
La	230	3174	151	29756
Lu	1	4	8	12
Mg	3815	446	43	124883
Mn	319	279	29	4912
Nb	58	80	179	733
Nd	250	1676	205	14145
Ni	2	0	0	28
Pb	884	383	161	1462
Pr	63	521	48	4591
Rb	93	1	0	1419
Sc	7	11	3	55
Sm	57	254	68	2065
Sr	15	85	6	2683
Ta	1	4	21	4
Tb	7	21	13	121
Th	22931	1328	4441	259370
Ti	1265	1621	5051	28133
Tm	2	5	9	15
U	829	551	489	6117
V	7	7	10	173
Y	147	413	653	2382
Yb	9	32	60	81
Zr	2160	1124	513	40623
ΣREE	1735	13281	2021	95919

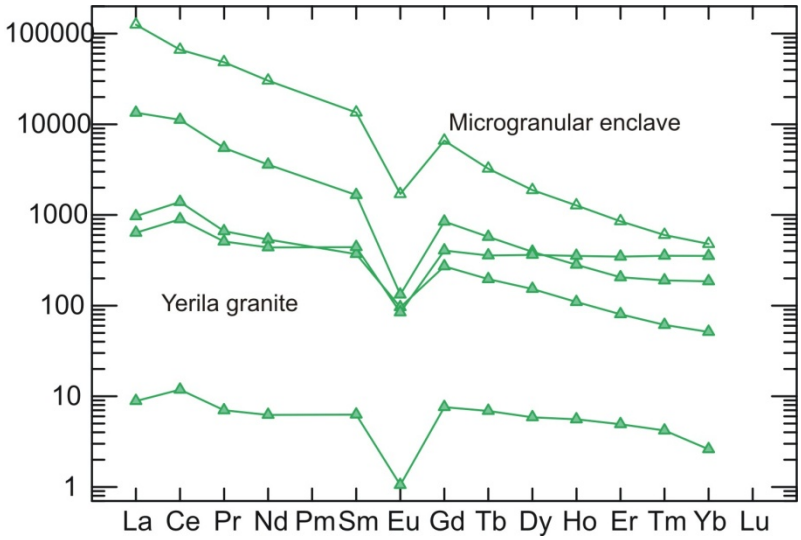

Figure 3.21 Rare earth element concentrations of U-Th minerals from MP Yerila granite and microgranular enclave normalised to chondrite values (Sun and McDonald, 1989).

The whole rock geochemistry of the HHP mafic and felsic rocks is mainly controlled by the behaviour of accessory minerals (Figure 3.22a to h). The presence, absence and modal abundance of allanite, zircon, Ti-mineral, apatite and U-Th minerals can be used to charcterise the whole rocks. The REE patterns in major and accessory minerals can be used to indicate the degree of fractionation progress in the HHP mafic and felsic rocks.

Figure 3.23a to d show relationship of trace elements (Th, Ce, U and La) in allanite from the Yerila and it enclaves and the Mt Painter whole rocks. The diagrams display positive trends, in which the Th, Ce, La and U concentrations for the Yerila Granite and it's enclaves plot between allanite and the whole rock analyses of other mafic and felsic rocks. This evidence suggests that high concentrations of trace elements such as Th, U, Ce and La in the Yerila Granite and it's enclave resulted from an abundance of allantites in them. In Y versus U and Th diagram, zircons from the HHP granitic and associated rocks and the whole rocks also show positive trends (Figure 3.24a and b).

The allanite with high Th, U, Ce, and La concentrations and the zircons with high Y, U and Th concentrations, possibly crystallized during interaction between mantle-derived magma and assimilated crust or mixing of mafic and felsic magma, has been picked up by the Yerila granite during its crystallization. Without over accessing allanite, the trace element

concentration of in the Yerila Granite could possibly be same amount of the other mafic and felsic rocks of the Mt Painter Province.

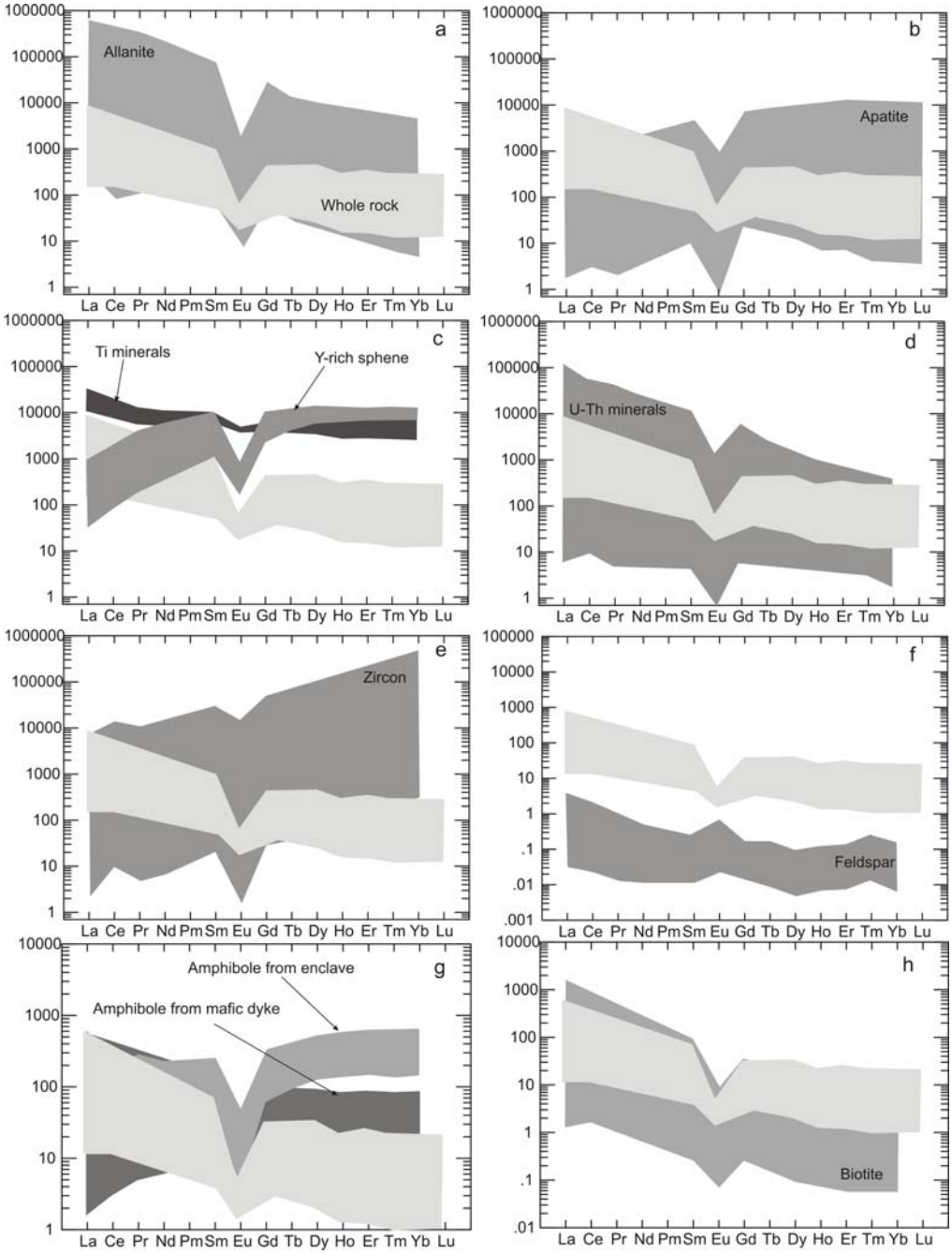

Figure 3.22a to h Rare earth element patterns of major and accessory minerals comparing to whole rocks of the Mt Painter rocks.

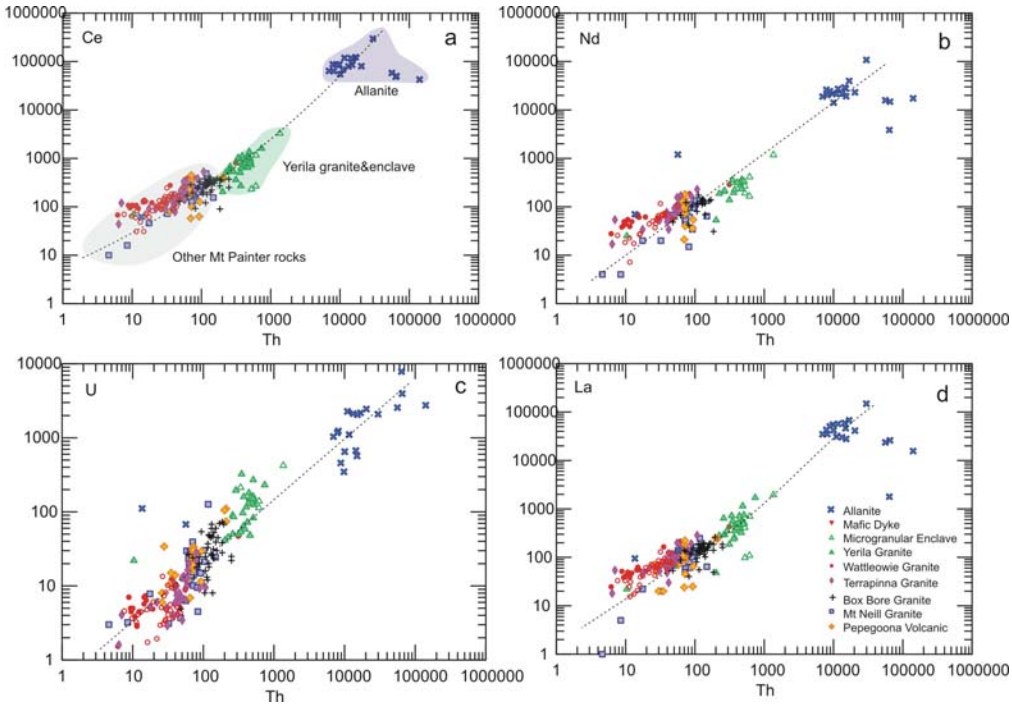

Figure 3.23 Binary diagram of trace elements concentrations of the whole-rock HHP mafic and felsic rocks and allanites from the Yerila Granite and microgranular enclaves of the Mt Painter Province a) Ce versus Th; b) Nd versus Th; c) U versus Th; d) La versus Th.

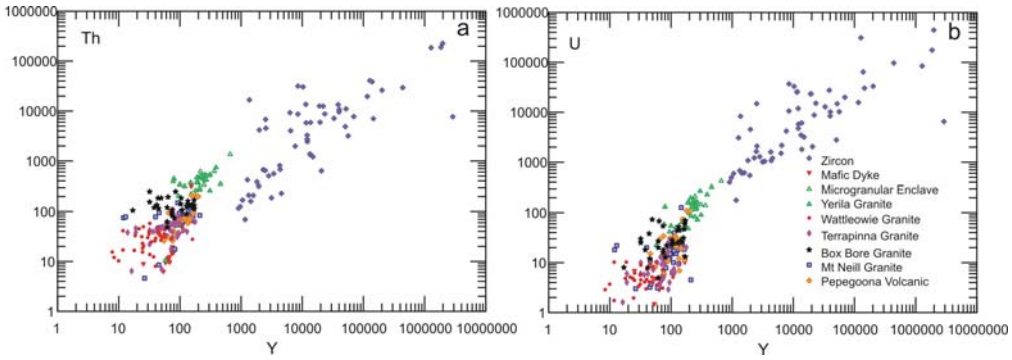

Figure 3.24 Binary diagram of U and Th concentrations of the HHP mafic and felsic whole rocks and zircons of the Mt Painter Province a) Th versus Y; b) U versus Y.